AD-A052 417 TEXAS A AND M UNIV COLLEGE STATION F/G 20/4
THE DEVELOPMENT AND APPLICATION OF A SIMPLE METHOD FOR DETERMIN--ETC(U)
FEB 78 B M RAO, V ELCHURI, P R SCHATZLE DAHC04-74-G-0184
UNCLASSIFIED ARO-11695.2-E NL

1 OF 2
AD
A052417

ARO 11695.2-E

12

a report

from the Texas A&M
RESEARCH FOUNDATION

College Station, Texas

SECURITY CLASSIFICATION OF THIS PAGE (When Data Entered)

REPORT DOCUMENTATION PAGE

READ INSTRUCTIONS BEFORE COMPLETING FORM

1. REPORT NUMBER: ~~TAMURF-ARO-1978-1~~
2. GOVT ACCESSION NO.
3. RECIPIENT'S CATALOG NUMBER

4. TITLE (and Subtitle): THE DEVELOPMENT AND APPLICATION OF A SIMPLE METHOD FOR DETERMINING UNSTEADY AIRLOADS IN SUBSONIC COMPRESSIBLE FLOW.

5. TYPE OF REPORT & PERIOD COVERED: Final Technical Report, 1 Jun 74 - 31 Dec 77

6. PERFORMING ORG. REPORT NUMBER

7. AUTHOR(s): Balusu M. Rao, Vijayvardhan Elchuri, Paul R. Schatzle, Larry J. McQuien

8. CONTRACT OR GRANT NUMBER(s): DAHC04-74-G-0184, DAAG29-76-G-0241

9. PERFORMING ORGANIZATION NAME AND ADDRESS: Texas A&M Research Foundation, F E Box H, College Station, Texas 77843

10. PROGRAM ELEMENT, PROJECT, TASK AREA & WORK UNIT NUMBERS: Army Regulation 70-5 Grants to Nonprofit Organizations .....

11. CONTROLLING OFFICE NAME AND ADDRESS: U.S. ARMY RESEARCH OFFICE, P.O. Box 12211, Research Triangle Park, NC 27709

12. REPORT DATE: Feb 78

13. NUMBER OF PAGES: 100 Pp 96

14. MONITORING AGENCY NAME & ADDRESS (if different from Controlling Office): ARO 11695.2-E

15. SECURITY CLASS. (of this report): unclassified

15a. DECLASSIFICATION/DOWNGRADING SCHEDULE

16. DISTRIBUTION STATEMENT (of this Report)

Approved for public release; distribution unlimited

17. DISTRIBUTION STATEMENT (of the abstract entered in Block 20, if different from Report)

18. SUPPLEMENTARY NOTES

The findings in this report are not to be construed as an official Department of the Army position, unless so designated by other authorized documents.

19. KEY WORDS (Continue on reverse side if necessary and identify by block number)

Aerodynamics; Unsteady Aerodynamics; Aeroelasticity; Helicopter Rotors; Hover

20. ABSTRACT (Continue on reverse side if necessary and identify by block number)

A numerical lifting surface method based on velocity potential formulation is applied for predicing aerodynamic loads in steady and unsteady flows for fixed and as well as rotary wings. The theory and the numerical procedures are validated by comparing with other analytical and experimental results. The techniques developed ~~are~~ resulted in a very efficient computational schemes.

DD FORM 1 JAN 73 1473 *EDITION OF 1 NOV 65 IS OBSOLETE

347350

SECURITY CLASSIFICATION OF THIS PAGE (When Data Entered)

THE DEVELOPMENT AND APPLICATION OF A SIMPLE METHOD FOR DETERMINING UNSTEADY AIRLOADS IN SUBSONIC COMPRESSIBLE FLOW

FINAL TECHNICAL REPORT
~~TAMURP-ARO-1978-1~~

Balusu M. Rao
Vijayvardhan Elchuri
Paul R. Schatzle
Larry J. McQuien

February 1978

DEPARTMENT OF THE ARMY
U.S. ARMY RESEARCH OFFICE
P.O. Box 12211
Research Triangle Park, NC 27709

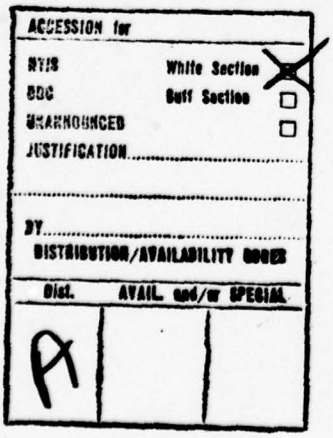

Grants: DAHC04-74-G-0184
DAAG29-76-G-0241

Texas A&M Research Foundation
F E Box H
College Station, Texas 77843

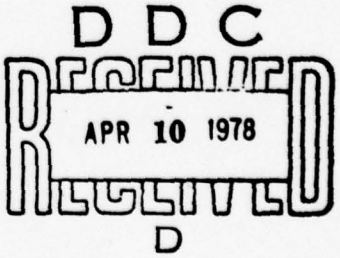

PREFACE

This final technical report was prepared by the Texas A&M Research Foundation under Grants DAHC04-74-G-0184 (1 June 1974 - 10 June 1976) and DAAG29-76-G-0241 (11 June 1976 - 31 December 1977). These grants were the follow on efforts after Project Themis.

In the summer of 1968, the U.S. Department of Defense through the U.S. Army Research Office at Durham sponsored a program of research on Aircraft Dynamics for Subsonic Flight at Texas A&M University. The work was funded under Project Themis (Contract DAHC04-69-C-0015) which had been established a year earlier in response to the late President Johnson's request that each Federal Agency should help to develop new centers of excellence in areas relevant to its goals. By means of Project Themis, the Department of Defense hoped to meet in part its long-term research needs, strengthen more of the nation's universities, increase the number of institutions performing research of high quality and achieve a wider distribution of research funds. In this way, it planned to enhance the United States' academic capabilities in science and technology.

After Project Themis expired in May 1973, Army Research Office awarded another Grant DA-ARO-D-31-124-71 G153 which was followed by the present grants. Dr. James J. Murray was the Technical Monitor for Project Themis efforts. Dr. Robert E. Singleton was the Technical Monitor for the present effort. Dr. W. P. Jones was the Program Manager for Project Themis, and later, was one of the Co-Principal Investigators along with the senior author of this report till he retired from Texas A&M University in August 1975. At that time, B. M. Rao became the Principal Investigator for the grants.

Texas A&M University benefited greatly from this entire program sponsored

by the Army Research Office to support our research work with a view to developing a center of excellence for the study of aerodynamic and dynamic problems of aircrafts and helicopters. Before this program, the University did not have an active research participation in this field. During this period, more than twenty students who worked in these research projects received their graduate degrees (Master's and Ph.D.'s). Several of these students are presently working for the Aerospace industry and the U. S. Government. During the same period, some of these students won awards for their outstanding research papers in AIAA Annual Regional and National Paper Competitions. This long-term funding from the Army Research Office has had a two-fold effect: first, some basic aerodynamic, efficient computational programs have been developed, and are being used by scientists in the field. Secondly, several students have received excellent educational training and research experience working in the sponsored research projects under professional engineers.

The authors gratefully acknowledge Dr. Robert E. Singleton for his sustained interest in the program, and for his encouragement and cooperation throughout the present grant period.

TABLE OF CONTENTS

LIST OF FIGURES

I. INTRODUCTION

Although man has been flying aircrafts for many years, a sizeable range of problems continue to exist. This is due partly to the appearance of new vehicles such as V/STOL aircraft and partly to the changes in the aircrafts' operational requirements. Hazen[1] emphasized the need for devoting greater effort to the study of subsonic aerodynamics. He noted that most current problems are dynamic in nature, and are concerned with aircraft maneuverability, response to atmospheric turbulence, aeroelastic phenomena and non-linear aerodynamic problems arising from separated flows. A better understanding of these problems is hinged upon the availability of efficient and accurate airloads prediction techniques for lifting surfaces. Comprehensive literature survey for the steady subsonic lifting line and lifting surface theories is presented in reference 2, and a brief summary of this survey follows.

One most basic approach in predicting spanwise loads on subsonic, three-dimensional wings is the lifting line technique due to Prandtl[3] which is applicable to large aspect ratio unswept planforms. The wing is represented by a bound vortex at the quarter chord, and a trailing vortex sheet extending from the bound vortex to infinity. The analysis is based on the assumption that at every point along the span the flow is essentially two-dimensional: the induced angle of attack produced by the trailing vortex wake is used to correct the two-dimensional lift of the bound vortex to account for the finite wing. The Prandtl lifting line concept does not produce the chordwise pressure distribution and is certainly limited by restrictions on wing planform.

Weissinger[3] extended Prandtl's lifting line concept to swept wings by modifying the straight bound vortex to a V-shaped vortex at the quarter

chord of the wing. In this technique, known as the Weissinger-L method, the velocity induced at the three-quarter chord by the trailing wake system and the inclined bound vortex pair is equated to the component of free stream velocity normal to the wing surface. This specification is justified by the fact that in two-dimensional theory this arrangement yields the correct circulation. An interesting variation of the Weissinger-L approach is a finite element method by Campbell[4], in which the swept bound vortex pair and the trailing wake are approximated by a system of rectangular horseshoe vortices arranged with their midpoints along the quarter chord. This approach is extended by Blackwell[5] to wing-tail combinations and to wings with pylons and end plates.

Although the lifting line methods predict the spanwise loading accurately for wings of conventional planforms, the extremes of sweep, taper and aspect ratios encountered in modern lifting surface design, along with a need for a complete description of the surface load distribution have resulted in the development of the lifting surface theories. The lifting surface problem has been approached approximately by multiple lifting-line and discrete loading element schemes. The direct approach[6,7,8] employs a series substitution in the governing integral equations relating the normal velocities on the surface to the pressure load, or an equivalent quantity across the surface. The series is derived from subsonic thin airfoil theory for chordwise loading and from the lifting line approach for spanwise loading. The series substitution allows evaluation of the lifting surface integral equation at a number of surface points equal to the desired number of series coefficients, or for a larger number of surface points in a 'least squares' sense.

Falkner[9] conceived the discrete loading element scheme in which the lifting surface is replaced by a system of concentrated horseshoe vortices,

and their strengths computed by satisfying the tangential flow condition at surface points equal in number to the unknown circulations. High speed digital computers have enabled investigators to refine the discrete loading element concept to allow solutions for larger systems of complex geometries. Woodward[10] represents an arbitrary wing-body combination in steady motion by a system of source doublet and vortex singularities. Lift and volume effects of the body are effected by line singularities along the body axis, while wing lift and wing-body interference are represented by planar singularities over a finite number of quadrilateral panels on the wing and interface region of the body. The strengths of the singularities are approximated as constant over each panel and determined so as to satisfy flow tangency.

The problems of unsteady flows have been studied by several investigators. Analytical/numerical solutions of the governing equations of motion are obtained by requiring that these solutions satisfy the appropriate boundary conditions. A brief literature survey is presented in reference 11. Recently, discrete or finite element schemes have been developed for oscillatory subsonic flows with good success, but these schemes include several approximations to facilitate solution of the complex mathematical formulations. Albano and Rodden[12], and Kalman et al[13] have demonstrated a wide variety of applications of the doublet-lattice method which is an extension of the vortex-lattice method of Falkner for unsteady flows. In this technique, the lifting surface to be analyzed is divided into a large number of planar panels. Each panel is then replaced by a horseshoe vortex representing the steady portion of the flow, and an oscillatory doublet distribution representing the unsteady part of the flow. The collocation method is then used to solve for the vortex and the doublet strengths incorporating the appropriate

boundary conditions. Reference 12 includes the analysis of an oscillating airfoil, an airfoil in an oscillating flow, and variable geometry wings with and without flaps while in reference 13, the doublet lattice method has been used to analyze non-planar configurations such as T-tail, a wing with end plates, and annular wings. This method is very restricted in its applications to non-planar configurations such as wing-body combinations. As each doublet panel has associated with it a trailing wake which extends infinitely aftward in a direction parallel to the free stream, the placement of panels on a body cannot be such as would allow the trailing wake of any panel to penetrate the body, for, this would constitute a physically unrealistic situation. Thus a body representation is generally restricted to being an annular wing of constant cross section without any inclination to the flow.

The analysis of a cascade of blades in unsteady flows has played an important role in compressor and turbine blade design. Chang and Chu[14] have analyzed a cascade of blades in synchronized oscillations. Their solution involved a modified form of Theodorsen's function which reduced to Theodorsen's function as the gap between two adjacent airfoils became infinite. Another approach by Schorr and Reddy[15] has been used to analyze the oscillatory flow over cascades with varying solidity and stagger angle. In their analysis, the airfoils in the cascade are replaced by a distribution of vortices and source-sink pairs whose strengths are determined for the appropriate boundary conditions. Since the formulation is very complicated, they are able to obtain only an approximate solution by replacing the kernel function with a polynomial.

Jones and Moore[16], and Rao and Jones[17] solved the problems of a cascade of oscillating airfoils in incompressible flow and oscillating

incompressible flow over a cascade of airfoils, respectively. They used the present lifting surface method based upon the velocity potential formulation, and were able to develop a very efficient computational scheme as an alternative to the existing lifting surface methods based on acceleration potential formulation.

The problem of wind-tunnel wall interference effects on oscillating airfoils in subsonic flow constitutes a special case of the blade-row problem, namely, the case in which stagger angle is zero and adjacent blade angles are 180° out of phase. Runyan and Watkins[18] treated the effect of wind-tunnel walls on the aerodynamic forces of an oscillating airfoil in a subsonic compressible flow. They simulated the walls by placing images at appropriate distances above and below the wings such that the condition of zero normal velocity at the tunnel walls is satisfied. In their formulation, the integral equation between the downwash and the oscillatory doublet strength involved a series of Hankel functions. The solution of this resulting equation yields the oscillatory doublet strength as a function of chordwise location on the airfoil and these doublet strengths were used to obtain acceleration potentials and hence the pressure distribution on the airfoil. An important result shown was that, for certain conditions of frequency, tunnel height, Mach number, the tunnel and wing may form a resonant system so that the forces on the wing are greatly changed from the condition of no tunnel walls.

Jones[19], independently developed a theory for estimating the effect of wind-tunnel walls on the airforces acting on an airfoil oscillating in a subsonic airstream. In his formulation, the integral equation between the downwash and the doublet strength (modified velocity potential) was essentially similar to the equation developed by Runyan and Watkins. Jones

summed the series of Hankel functions in the integral and developed a numerical procedure applicable to the low frequency values. The results obtained for a special case compared well with available experimental results.

Lane and Friedman[20] developed a method for calculating the aerodynamic forces experienced by a cascade with arbitrary stagger and interblade phase-lag angles. Their method utilized Fourier transforms of blade pressure-jump functions which permit the kernel function, appearing in the integral equation relating the upwash to the pressure-jump transform, to be expressed in a closed form, by assuming a commonly used trigonometric series expansion involving Bessel functions. However, their solution involved a very complicated and a tedious computational procedure. They demonstrated that the resonance condition similar to that of the wind-tunnel wall interference problem, may occur in staggered cascades with arbitrary interblade phase-lag, the resonance parameter values depending upon Mach number, oscillatory frequency, interblade phase-lag, gap, stagger, and acoustic velocity.

Fleeter[21] studied the effects of compressibility on both fluctuating lift and the fluctuating moment coefficients for cascaded airfoils due to an upstream nonuniformity. Through the application of Fourier transform theory, Fleeter reduced, the time-dependent, compressible, two-dimensional partial differential equation which describes the perturbation velocity potential, into an integral solution equation. Although the details of the solution were not given in the paper, Fleeter seems to have adopted the laborious procedure used by Lane and Friedman.[20]

Kaji and Okazaki[22] investigated the problem of propagation of sound waves through a blade row using the acceleration potential method. They made use of the singular point method in a rigorous and general form, in which the kernel function of the aerodynamic integral is expressed by a

rapidly convergent series of exponential functions.

Rao and Jones[23] adopted the present lifting surface technique for determining the airload and moment coefficients on a typical airfoil of a staggered cascade of airfoils in subsonic flow. Circumferential distortion due to inflow conditions is expressed as an interblade phase-lag, and both oscillatory inflow and the case of oscillating blades are considered. Results are obtained for several values of frequency, Mach number, and interblade spacing, stagger, and phase-lags. The results of the oscillatory flow case compare well with those of Fleeter.[21]

Runyan and Woolston[24] solved for the aerodynamic loads on oscillating wings by modifying the concepts of Falkner[9] for steady lifting surface theory. The loading on the wing was determined by solving a set of simultaneous equations that were generated by representing the loading with a series representation compatible with boundary conditions. In another approach, Lawrence and Gerber[25] simplified the governing equations by using the assumption of low aspect ratio. They approximated the velocity potential equation by using a weighting factor in the integral, and then replacing the integrals with approximate functions. Comparison with the results of references 26 and 27 indicated that the Lawrence and Gerber method was only valid for wings with aspect ratio less than 4. The main disadvantage of the method is that it cannot predict the pressure distribution. Dengler and Goland[28] extended the lifting line formulation of Weissinger to the oscillatory case. Their method is much simpler mathematically than lifting-surface methods; however, the chordwise pressure distribution cannot be predicted.

The pressure distribution measured for pitching and vertical oscillations of low aspect ratio wings by Laidlaw and Halfman[29] were compared to the

results of Lawrence and Gerber[25]. This comparison verified the validity of Lawrence and Gerber method for low aspect ratio wings.

The references cited above have adopted the kernel function representation and have illustrated several disadvantages. First, the complexity of the kernel function involved in the integral equation necessitates approximations to obtain a solution. Second, the kernel function method is difficult to use numerically because of the singularities and rapid variations near the leading edge of the airfoil. On the other hand, the present lifting surface method based on the velocity potential formulation is conceptually very simple, and hence can be adapted to any arbitrary planar thin surface(s). Also, in the case of compressible flow, the area integration can be replaced by line integration with the aid of Biot-Savart's law, thereby reducing the computational time substantially. Unlike the kernel function method, the present lifting surface technique deals with the circulation which is more suitable for numerical solutions.

The discussion so far has been limited to the application of lifting surface methods to two-dimensional and three-dimensional rectilinear flows. What follows is a brief account of the unsteady airloads prediction methods for helicopter rotor blades.

More papers have been published on the subject of unsteady aerodynamics of rotor blades during the past few years than in all the earlier years of the helicopter development. In earlier work, attention was focused on vibration problems which often limit helicopter performance. With the advent of high speed helicopters, it has also become important to study the compressibility effects and the blade flutter problems. Jones et al[30] gave a detailed account of significant developments in the field of unsteady aerodynamics of helicopter rotor blades. Specifically, the latest advances

in such problem areas as stall flutter of a retreating rotor blade, flutter of the advancing blade, transient effects due to the interaction of the tip-vortex of one blade with a following blade and wake induced instabilities in hovering and low-speed flight, were discussed.

Problem areas of blade loading and the transient effects due to blade interaction with the wakes of other blades and the flutter characteristics of the advancing blade are considered here. It has been found that under certain operating conditions, rotor blades can flutter in both hovering and forward flight. This phenomenon has been investigated by several researchers and their studies are of particular interest. It has been known for a long time that the proximity of the helical wake is a contributing factor to blade flutter. When the rotor has high inflow through the disk, the wake of a blade is removed rapidly away and its effect on the aerodynamic forces on the blade is approximately the same as that of a rectilinear wake. For the case of low inflow, the wake is closely coiled under the rotor disk and it can have a strong influence on the aerodynamic forces acting on a blade. For low inflow conditions, Loewy[31] used a simplified mathematical model of the flow and developed a general theory. He was able to derive formulae for the aerodynamic forces on a typical blade section as a function of reduced frequency, the frequency ratio, and wake spacing. The special function that he obtained was similar to that of Theodorsen's function for a single airfoil in straight flow. He has shown that the airloads are highly oscillatory for the smaller values of wake spacing. Since the stability of the rotor blade depends on its aerodynamic coefficients, Loewy also investigated the variation in the pitching moment damping coefficient of a particular blade section as the frequency ratio, p/Ω, varied for specified positions of axis of oscillation and a range of values of wake spacing. He found that the damping

coefficient became negative whenever p/Ω was slightly greater than an integer for axis oscillation either forward or aft of quarter-chord. Similarly, he found that the damping coefficient for a flapping oscillation dropped sharply at integral values of p/Ω but did not actually become negative. From these results, he concluded that at low inflow, wake-excited pitching oscillations of the blade might occur when the frequency ratio is approximately an integer and the pitch-axis is not at quarter-chord.

Whereas Loewy developed his theory for a multibladed rotor, J. P. Jones[32] had independently treated the simpler case of a single rotating blade in hovering flight. He applied a method developed by W. P. Jones[33] to derive the appropriate aerodynamic coefficients for an oscillating single rotor blade for use in his flutter analysis. He approximated the actual flow conditions by neglecting curvature effects and assuming a simple two-dimensional mathematical model consisting of a reference blade and its wake and an infinite number of wakes lying beneath the reference blade extending from $-\infty$ to ∞. He considered flapping and pitching motions and compared his results with those obtained experimentally by Daughaday and Kline[34]. On the basis of this work, it was concluded that the wake is primarily responsible for some of the vibratory phenomena found on helicopters in practice.

Timman and Van de Vooren[35], on the other hand, assumed that there was no inflow through the rotor disk and developed a theory for calculating the aerodynamic forces on a blade rotating through its own wake. Their results agree with those obtained by Loewy[31] and Jones[32] in the limit when zero spacing between the wakes is assumed. Flutter calculations were done for a two-bladed rotor model and their predictions were compared with experimental observations. They found that wake induced flutter could occur under

certain conditions. When the inertia axis of the blade is aft of its pitching axis, wake flutter is possible if the natural flapping frequency is larger than the natural pitching frequency. Conversely, when the inertia axis is forward, the pitching frequency has to be higher than the flapping frequency for flutter to occur. All this theoretical work confirms the conclusion that the proximity of the wake is a contributing factor to rotor blade flutter.

All the theoretical work described above is based on the assumption that the flow is incompressible. However, with the advent of helicopters capable of flying with blade tip speeds ranging up to and in excess of the speed of sound, compressibility effects need to be taken into account when determining aerodynamic coefficients for use in flutter analysis. Jones and Rao[36] were able to do this and have computed aerodynamic coefficients for a range of Mach numbers, reduced frequencies, and wake spacing. Their analysis is based on the application of the theory of Jones[37], for a single airfoil oscillating in compressible flow, to the Loewy two-dimensional mathematical model of the helical wake. The values of the aerodynamic coefficients agree with those obtained by Loewy[31] and J. P. Jones[32] for zero Mach number but differ appreciably as the Mach number is varied.

Hammond[38] also developed a theory for determining compressibility effects by using a different model of flow from that used in Ref. 36. In his model, the wake of the qth blade of a Q bladed rotor after n revolutions extends from $-2\pi(n+q/Q)$ to ∞; in Jones and Rao's model it extends from $-\infty$ to ∞. His aerodynamic coefficients for several Mach number and inflow ratios are in general agreement with the results of Jones and Rao.

While the aerodynamic derivatives predicted by two-dimensional strip

theory are widely used in predicting the flutter speeds of helicopter rotor blades, the method does not allow for curvature and finite aspect ratio effects. For incompressible flow, Ashley et al in Ref. 39 developed a three-dimensional model in which they modified Reissner's theory[40] for oscillating wings in rectilinear flow by including the free stream velocity variations along the span. Their results indicate a negligible difference between two and three-dimensional solutions up to 95% of the span. Jones and Rao[41] also studied tip-vortex effects in compressible flow and they also concluded that such effects are negligible except in regions close to the tip.

The earlier attempts to include the tip vortices in a truly three-dimensional fashion involved a helical wake representation below the rotor blade in hover flight and a skewed helical pattern for forward flight. Miller[42] summarized some of the work that has been done at M.I.T. and elsewhere up to that time on the prediction of unsteady airloads on helicopter rotor blades. He showed that by replacing the curved tip vortex from the preceding by a straight line vortex which is tangential to the tip vortex at the point where it crosses under a following blade, he could obtain reasonable estimations of its effect. It was pointed out that almost all the harmonic content of the blade air load of interest in rotor vibration is that contained in harmonics above the second. By representing the oscillatory wake of the blade itself in a relatively simple way and treating the tip vortex of the preceding blade, he was able to obtain reasonable results.

In some of his earlier work, Miller[43,44] developed a helical wake model in which the rotor wake was divided into a "near" wake and a "far" wake. The near wake included the portion attached to the blade that

extends approximately one-quarter of a revolution from the blade trailing edge. The effects of the near wake include an induced chordwise variation in downwash and were formulated using an adaptation of Loewy's strip theory. The chordwise variation in the velocity over the airfoil induced by the far wake was neglected. Miller extended his model to study the forward flight case and found that the nonuniform downwash induced at the rotor disk by the wake vortex system could account for the higher harmonic airloads encountered on rotor blades in forward flight. He also showed that under certain conditions of low inflow and low speed transition flight the returning wake could be sucked up into the leading edge of the rotor which would account for some of the vibration and noise.

Several investigators used better representations of the helical or skewed helical wake for steady flight. Jenney et al[45] reviewed several simpler conventional methods for computing hover performance and pointed out that one of the primary reasons for discrepancies in results are due to the use of inadequate mathematical wake models in the conventional theories. They attributed the major discrepancies to wake contraction in close proximity to the rotor. They developed a theoretical lifting line Hover Performance method representing the wake by a finite number of vortex filaments. They prescribed the wake geometry in the computer program in which provisions were made to include a wide variety of wake geometries ranging from the classical uncontracted, momentum axial velocity geometry (classical wake) to the more realistic contracted, variable-axial-velocity geometry.

Landgrebe[46],[47] subsequently, conducted an analytical and experimental investigation to acquire systematic model rotor performance and wake geometry data and to evaluate the accuracy of various analytical methods in

predicting the effects on performance of changes in helicopter rotor design and operating parameters. A rapid computer analysis was developed for computing the distorted wake geometry of a rotor wake. The numerical procedure involved two basic steps - the use of the Biot-Savart law to compute the wake distortion velocities produced by a given wake geometry and the integration of these velocities over a small time increment to establish new wake geometry. These steps were successively repeated until a converged periodic wake geometry resulted. It was found that analysis based on a contracted wake geometry generally provided significantly improved predictions of performance for those rotor operating conditions where the more classical uncontracted wake analyses exhibited major shortcomings. Through extensive correlation testing, he validated the general trends predicted by his numerical work. Analysis of the wake data for that portion of the wake which was stable (i.e. near the rotor) indicated that the data could be expressed in relatively simple generalized equations which facilitate the rapid estimation of contracted wake geometries for a wide range of rotor design and operating conditions.

In an independent study, Piziali[48], developed an alternative numerical method in which the wake of the rotor blade is represented by discrete straight lines and trailing vortex elements. He satisfied the chordwise boundary conditions, but the rotor blade was limited to one degree-of-freedom in flapping. His method is also limited by the use of empirical factors which adjusts the discrete time positioning of the shed vortices.

Sadler[49], using a model similar to that of Piziali, developed a method for predicting the helicopter wake geometry at a "start up" configuration. He represented the wake by a fine mesh of transverse and trailing vortices starting with the first movement of the rotor blade generating a bound vortex, and, to preserve zero total vorticity, a corresponding shed

vortex in the wake. Integrating the mutual inteference of the trailing and shed vortices upon each other over small intervals of time, Sadler was able to predict a wake geometry. Although his model showed fair agreement with the available experimental data for advance ratios above one-tenth, Sadler's method is limited due to the large computational time required to represent the wake by a finite mesh.

Another important problem is the prediction of the unsteady airloads in normal forward flight and allowing for blade-tip vortex interaction. Landgrebe and other investigators demonstrated that as a given blade advances the tip vortex from the preceding blade may pass closely underneath it and the point of intersection moves inward along the blade as Ψ increases. Ward and Snyder[50] predicted the extent of the inward movement as a function of the advance ratio and the number of blades. In their study, they did not account for the actual induced response due to the movement of the tip vortex but instead considered the analogous problem of the response of the blade to a repetitive moving load. Their results showed for flight at high advance ratios (μ>0.25) the main effect of the moving load was to amplify response in the lower resonance modes.

The topic of the evaluation of appropriate aerodynamic coefficients for use in the analysis of classical bending-torsion flutter of rotor blades is of great interest to a helicopter designer in view of the present day helicopters with high tip speeds. Shipman and Wood[51] considered this problem but they did not take compressibility and finite aspect ratio effects into account. The two-dimensional mathematical model used was similar to that employed by other authors except that they assumed that flutter would first occur when the relative velocity over the rotor blade reaches its critical value when $\Psi = \pi/2$. For greater or lower values of

Ψ, the realtive speed would be reduced below the critical speed for flutter and any incipient growing flutter oscillation would be damped. This reasoning led them to represent the blade motion by a series of oscillatory pulses, where each disturbance occurs over the range, $\pi/2 - \Delta\Psi_1 < \Psi < \pi/2 - \Delta\Psi_2$. Corresponding to each burst of oscillation, packets of vorticity are assumed to be shed in the wake. With increasing forward speed, the spacing between the packets of vorticity also increases and it was found that the flutter speed became constant when μ, the advance ratio, was above 0.2.

The approach used in a study by Rao and Jones[52] differs from that adopted by Shipman and Wood in that continuous high frequency small oscillations are assumed to be superimposed on the normal periodic motion of the blade. Rao and Jones developed a simple but general numerical lifting surface method for predicting unsteady airloads on a single-bladed rotor blade on a full three-dimensional basis. The numerical method was based on the velocity potential formulation and was not restricted in any way as to frequency, mode of oscillation or aspect ratio when $M < 1$. However, in their model they used a classical wake model and considered uniform downwash only. The general theory was developed for a rotor blade at the $\Psi = \pi/2$ position where flutter is most likely to occur. Calculations of aerodynamic coefficients for use in flutter analysis were made for forward and hovering flight with low inflow for Mach numbers 0 and 0.8 and frequency ratios $p/\Omega = 1$ and 4. The results were compared with values given by two-dimensional strip theory for a rigid rotor hinged at its root. The comparisons indicated the inadequacies of strip theory for airload prediction. One important conclusion drawn from this study was that the curved wake has a substantial effect on the chordwise load distribution. The pitching moment aerodynamic coefficients differed appreciably from the results given by strip theory.

II. AERODYNAMIC THEORY

Governing Equation of Flow

Consider an airfoil in motion in a continuous fluid medium. A Cartesian coordinate system is chosen such that the origin O lies at the midchord point of the airfoil, and the positive x-axis in the direction of the free stream relative to the airfoil. The system of coordinates is shown in the sketch below.

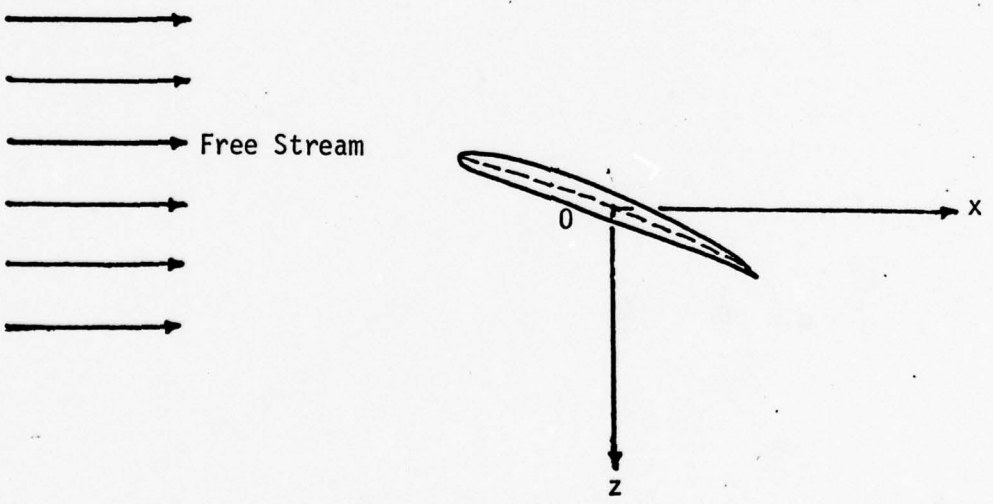

Velocity of a fluid particle at any point $P(x_p, y_p, z_p)$ in the flow field is

$$\vec{q} = q_x \hat{i} + q_y \hat{j} + q_z \hat{k} \quad . \tag{2.1}$$

In a potential flow around the airfoil, the laws of conservation of mass and momentum are, respectively,

$$\frac{D\rho}{Dt} + \rho \nabla \cdot \vec{q} = 0 \quad , \tag{2.2}$$

and

$$\frac{D\vec{q}}{Dt} + \frac{1}{\rho} \nabla p = \vec{0} \quad . \tag{2.3}$$

Expressing the velocity $\vec{q}$ in terms of a potential function ϕ_t, the continuity equation (2.2) reduces to

$$\nabla^2 \phi_t = -\frac{1}{\rho} \frac{D\rho}{Dt} \quad . \tag{2.4}$$

For a barotropic fluid, $p = p(\rho)$ and, hence

$$\nabla^2 \phi_t = -\frac{1}{\rho a^2} \frac{Dp}{Dt} \quad . \tag{2.5}$$

Along a streamline, the momentum equation yields

$$\frac{D}{Dt}\left(\frac{q^2}{2}\right) - \frac{1}{\rho} \frac{\partial p}{\partial t} = \frac{1}{\rho} \frac{Dp}{Dt} \quad . \tag{2.6}$$

Also, from the momentum equation,

$$\nabla \left[\frac{\partial^2 \phi_t}{\partial t^2} + \frac{\partial}{\partial t}\left(\frac{q^2}{2}\right) + \frac{1}{\rho} \frac{\partial p}{\partial t} \right] = 0 \tag{2.7}$$

Equations (2.5), (2.6) and (2.7) are combined to obtain the governing

potential flow equation,

$$\nabla^2 \phi_t - \frac{1}{a^2}\left[\frac{\partial^2 \phi_t}{\partial t^2} + \frac{\partial}{\partial t}(q^2) + \vec{q}\cdot\nabla\left(\frac{q^2}{2}\right)\right] = 0. \quad (2.8)$$

This general form of the equation is applicable to unsteady compressible flows with no shock waves. Based on the type of flow, equation (2.8) is modified as follows.

a. Incompressible Flow (Steady and Unsteady State).

Local speed of sound in an incompressible medium is infinite and hence the governing differential equation of potential flow becomes Laplace's equation,

$$\nabla^2 \phi_t = 0 . \quad (2.9)$$

b. Compressible Flow (Unsteady State).

Velocity of a fluid particle in the vicinity of the airfoil can be written as

$$\vec{q} = (U + u)\hat{i} + v\hat{j} + w\hat{k} , \quad (2.10)$$

where the perturbation velocity components u, v, and w are considered small in comparison to the free stream velocity component. Coordinate transformations

$$\left.\begin{aligned} x &= X\ell \\ y &= Y\ell/\beta \\ z &= Z\ell/\beta \\ t &= T\ell/U \end{aligned}\right\} \quad (2.11)$$

where, $\beta = \sqrt{1-M^2}$,

and the substitution

$$\phi = U\ell\,\Phi(X,Y,Z)\,e^{i(\lambda X + \omega T)} \tag{2.12}$$

modify equation (2.8) to

$$\nabla_*^2\,\Phi + \kappa^2\,\Phi = 0\ , \tag{2.13}$$

with

$$\nabla_*^2 \equiv \frac{\partial^2}{\partial X^2} + \frac{\partial^2}{\partial Y^2} + \frac{\partial^2}{\partial Z^2}\ , \tag{2.14}$$

$$\kappa = M\omega/\beta^2\ , \tag{2.15}$$

and

$$\lambda = M\kappa\ . \tag{2.16}$$

c. Compressible Flow (Steady State).

Frequency of external excitations p'=0 in the steady state resulting in κ=0, and the governing flow equation becomes Laplace's equation in the transformed coordinates,

$$\nabla_*^2\,\Phi = 0\ . \tag{2.17}$$

Velocity Potential in Terms of Boundary Values

To obtain a relation for the velocity potential Φ in terms of its value and the normal derivative on known boundaries so as to formulate a boundary value problem in conjunction with Helmholtz's equation (2.13), we now refer to the sketch.

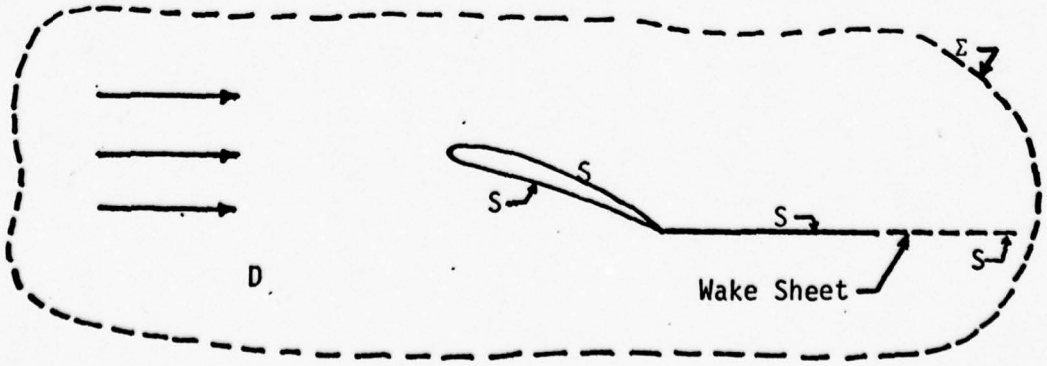

Fluid region D surrounding the airfoil is bounded externally by the surface Σ, and encloses an impermeable surface S comprising the airfoil and the attached wake surfaces.

With the use of Gauss' divergence theorem for the vector $\vec{B} = \Phi \nabla \Phi'$, a reciprocal theorem can be proved as

$$\iint_{S+\Sigma} \Phi \frac{\partial \Phi'}{\partial n} dS = \iint_{S+\Sigma} \Phi' \frac{\partial \Phi}{\partial n} dS \ , \tag{2.18}$$

where Φ and Φ' both satisfy Helmholtz's equation (2.13), and $\vec{n}$ represents the unit normal vector at any point on S and Σ, directed toward the fluid. Assuming $\Phi' = \exp(-i\kappa R)/R$ where R is the distance between a flow point $P(X_p, Y_p, Z_p)$ and a point $Q(X, Y, Z)$ on $(S + \Sigma)$. In order to avoid the singularity in Φ' when the points P and Q coincide, P is enclosed in a small spherical surface σ which, in the limit, is taken to the point P. Further, as the exterior boundary is extended toward infinity, contributions over Σ in equation (2.18) approach zero for point P in the vicinity of the airfoil. Equation (2.18) is now rewritten as

$$4\pi \Phi(X_p, Y_p, Z_p) = \iint_S \left[\Phi(X,Y,Z) \frac{\partial}{\partial n} \left(\frac{e^{-i\kappa R}}{R} \right) - \frac{e^{-i\kappa R}}{R} \cdot \frac{\partial}{\partial n} \Phi(X,Y,Z) \right] dS, \tag{2.19}$$

where X, Y, Z are the independent variables in the integrand on the right side. This equation provides a means to express the velocity potential Φ_p at any point P in the flow in terms of its value $\Phi(X,Y,Z)$ and the normal derivative $\partial\Phi/\partial n$ on the surface of the airfoil and its wake. With the assumption of thin airfoil, the closed surface of integration can be divided into two equal and parallel surfaces. Also, the

physical boundary condition on these surfaces requires the relative flow to follow the airfoil and its wake geometries. That is,

$$\vec{Q}\cdot\vec{n} = (\vec{q}/U)\cdot\vec{n} = (\hat{i} + \nabla\Phi)\cdot\vec{n} = 0 \quad , \tag{2.20}$$

whereby

$$\frac{\partial\Phi}{\partial n} = -n_x \quad . \tag{2.21}$$

It is further noted that on the upper surface of integration $\partial/\partial n_u \simeq -\partial/\partial Z$ and on the lower side $\partial/\partial n_\ell \simeq \partial/\partial Z$. Hence, from equation (2.19), the downwash induced at a point P on the airfoil in a direction along the positive z-axis is given by

$$4\pi \frac{\partial\Phi_p}{\partial Z_p} = 4\pi W_p = \iint_{\substack{\text{airfoil}\\+\\\text{wake}}} (\Phi_u - \Phi_\ell) \frac{\partial^2}{\partial Z_p^2}\left(\frac{e^{-i\kappa R}}{R}\right) dS \quad . \tag{2.22}$$

Rewriting,

$$4\pi W_p = \iint_{\substack{\text{airfoil}\\+\\\text{wake}}} K(X,Y,Z) \frac{\partial^2}{\partial Z_p^2}\left(\frac{e^{-i\kappa R}}{R}\right) dS \quad , \tag{2.23}$$

where $K = \Phi_u - \Phi_\ell$ defines the strength of the doublet distribution over the airfoil and wake surfaces.

Equation (2.23) is the most general form of the velocity potential formulation applicable to unsteady flow of a compressible fluid past a thin airfoil at small angles of attack. It can be suitably modified for incompressible flow (steady or unsteady), two-dimensional compressible flow (steady and unsteady) and three-dimensional steady compressible flow.

For all steady cases, and unsteady incompressible flow, $\kappa = 0$, and equation (2.23) becomes

$$4\pi W_p = \iint_{\substack{\text{airfoil}\\+\\\text{wake}}} K \frac{\partial^2}{\partial Z_p^2}\left(\frac{1}{R}\right) dS \quad . \tag{2.24}$$

For two-dimensional subsonic unsteady flow, the velocity potential formulation reduces to

$$2\pi W_p = \int_{-1}^{\infty}\int_{0}^{\infty} K(X,Z)\,\frac{\partial^2}{\partial Z_p^2}\left(\frac{e^{-i\kappa R}}{R}\right) dY dX \,, \tag{2.25}$$

where P is a point on the Y=0 axis, and

$$R = \left[(X-X_p)^2 + Y^2 + Z_p^2\right]^{1/2} . \tag{2.26}$$

Equation (2.25) is rearranged as

$$2\pi W_p = \int_{-1}^{\infty} K(X,Z)\left[\frac{\partial^2}{\partial Z_p^2}\int_{0}^{\infty}\frac{e^{-i\kappa R}}{R}\,dY\right] dX \,. \tag{2.27}$$

We now let

$$\left.\begin{aligned} \alpha^2 &= (X-X_p)^2 + Z_p^2 \,, \text{ and} \\ \alpha^2 + Y^2 &= \alpha^2\tau^2 \end{aligned}\right\} \tag{2.28}$$

whereby

$$2Y\,dY = 2\alpha^2\tau\,d\tau \,, \tag{2.29}$$

or

$$dY = \left\{\tau\alpha/\sqrt{\tau^2-1}\right\} d\tau \,. \tag{2.30}$$

Therefore,

$$\begin{aligned} \int_{0}^{\infty}\frac{e^{-i\kappa R}}{R}\,dY &= \int_{1}^{\infty}\frac{e^{-i\kappa\tau|\alpha|}}{\sqrt{\tau^2-1}}\,d\tau \\ &= -\frac{\pi i}{2}\,H_0^{(2)}(\kappa|\alpha|) \,, \end{aligned} \tag{2.31}$$

where

$$\left.\begin{aligned} |\alpha| &= \left[(X-X_p)^2 + Z_p^2\right]^{1/2}, \text{ and} \\ H_0^{(2)}(\kappa|\alpha|) &= J_0(\kappa|\alpha|) - i\,Y_0(\kappa|\alpha|) \,, \text{ is} \end{aligned}\right\} \tag{2.32}$$

the modified Hankel function of the second kind Use of result (2.31) in equation 2.27 yields

$$2\pi W_p = -\frac{\pi i}{2}\int_{-1}^{\infty} K(X,Z)\,\frac{\partial^2}{\partial Z_p^2}\left[H_0^{(2)}(\kappa|\alpha|)\right] dX \,. \tag{2.33}$$

The function $H_0^{(2)}(\kappa|\alpha|)$, defined by equation (2.32) satisfies the Bessel's equation

$$\frac{d^2}{d\mu^2} H_0^{(2)}(\mu) + \frac{1}{\mu} \frac{d}{d\mu} H_0^{(2)}(\mu) + H_0^{(2)}(\mu) = 0 , \tag{2.34}$$

where

$$\mu = \kappa|\alpha| . \tag{2.35}$$

Hence it can be shown that $H_0^{(2)}(\kappa|\alpha|)$ also satisfies the two-dimensional wave equation,

$$\left(\frac{\partial^2}{\partial X_p^2} + \frac{\partial^2}{\partial Z_p^2} + \kappa^2 \right) H_0^{(2)}(\kappa|\alpha|) = 0 . \tag{2.36}$$

To show this, we consider the following.

$$\left.\begin{aligned} H_0^{(2)} &= H_0^{(2)}(\mu) \quad , (\mu = \kappa|\alpha|) \\ \text{where} \quad \mu &= \mu(X_p, Z_p) \end{aligned}\right\} \tag{2.37}$$

$$\therefore \quad \frac{\partial}{\partial X_p} H_0^{(2)} = \frac{dH_0^{(2)}}{d\mu} \cdot \frac{\partial \mu}{\partial X_p} \quad , \text{ and} \tag{2.38}$$

$$\begin{aligned} \frac{\partial^2}{\partial X_p^2} H_0^{(2)} &= \frac{\partial}{\partial X_p} \left[\frac{dH_0^{(2)}}{d\mu} \cdot \frac{\partial \mu}{\partial X_p} \right] \\ &= \frac{d^2 H_0^{(2)}}{d\mu^2} \left(\frac{\partial \mu}{\partial X_p} \right)^2 + \frac{dH_0^{(2)}}{d\mu} \cdot \frac{\partial^2 \mu}{\partial X_p^2} . \end{aligned} \tag{2.39}$$

Also,

$$\frac{\partial \mu}{\partial X_p} = - \frac{\kappa^2 (X - X_p)}{\mu} . \tag{2.40}$$

Therefore,

$$\frac{\partial^2 \mu}{\partial X_p^2} = \frac{\kappa^2 (X - X_p)}{\mu^2} \left\{ - \frac{\kappa^2 (X - X_p)}{\mu} \right\} + \frac{\kappa^2}{\mu} \tag{2.41}$$

Substituting equations (2.40) and (2.41) in equation (2.39),

$$\frac{\partial^2}{\partial X_p^2} \left[H_0^{(2)}(\mu) \right] = \frac{d^2 H_0^{(2)}(\mu)}{d\mu^2} \left[\frac{\kappa^4 (X - X_p)^2}{\mu^2} \right] + \frac{dH_0^{(2)}(\mu)}{d\mu} \left[\frac{\kappa^2}{\mu} - \frac{\kappa^4 (X - X_p)^2}{\mu^3} \right] . \tag{2.42}$$

Similarly,

$$\frac{\partial}{\partial Z_p} \left[H_0^{(2)}(\mu) \right] = \frac{dH_0^{(2)}}{d\mu} \cdot \frac{\partial \mu}{\partial Z_p} , \tag{2.43}$$

and

$$\frac{\partial^2}{\partial Z_p^2} \left[H_0^{(2)}(\mu) \right] = \frac{\partial}{\partial Z_p} \left[\frac{dH_0^{(2)}}{d\mu} \cdot \frac{\partial \mu}{\partial Z_p} \right] = \frac{d^2 H_0^{(2)}}{d\mu^2} \left(\frac{\partial \mu}{\partial Z_p} \right)^2 + \frac{dH_0^{(2)}}{d\mu} \cdot \frac{\partial^2 \mu}{\partial Z_p^2} . \tag{2.44}$$

Now,

$$\left. \begin{aligned} \frac{\partial \mu}{\partial Z_p} &= \frac{\kappa^2 Z_p}{\mu} \quad , \text{ and} \\ \frac{\partial^2 \mu}{\partial Z_p^2} &= \frac{\kappa^2}{\mu} - \frac{\kappa^2 Z_p}{\mu^2} \left(\frac{\kappa^2 Z_p}{\mu} \right) . \end{aligned} \right\} \tag{2.45}$$

Therefore

$$\frac{\partial^2}{\partial Z_p^2}\left[H_0^{(2)}(\mu)\right] = \frac{d^2H_0^{(2)}}{d\mu^2}\left[\frac{\kappa^4 Z_p^2}{\mu^2}\right] + \frac{dH_0^{(2)}}{d\mu}\left[\frac{\kappa^2}{\mu} - \frac{\kappa^4 Z_p^2}{\mu^3}\right]. \quad (2.46)$$

Substituting equations (2.42) and (2.46) in equation (2.36), we have,

$$\left(\frac{\partial^2}{\partial X_p^2} + \frac{\partial^2}{\partial Z_p^2} + \kappa^2\right) H_0^{(2)}(\mu)$$

$$= \frac{d^2H_0^{(2)}}{d\mu^2}\left[\kappa^2\right] + \frac{dH_0^{(2)}}{d\mu}\left[\frac{2\kappa^2}{\mu} - \frac{\kappa^4\alpha^2}{\kappa^3\alpha^3}\right]$$

$$+ \kappa^2 H_0^{(2)}$$

$$= \kappa^2\left[\frac{d^2H_0^{(2)}}{d\mu^2} + \frac{1}{\mu}\frac{dH_0^{(2)}}{d\mu} + H_0^{(2)}\right]$$

$$= 0 \text{ , in view of the equation (2.34).}$$

Hence,

$$\frac{\partial^2}{\partial Z_p^2}\left[H_0^{(2)}(\kappa|\alpha|)\right] = -\left(\frac{\partial^2}{\partial X_p^2} + \kappa^2\right)\left[H_0^{(2)}(\kappa|\alpha|)\right], \quad (2.47)$$

whereby the formulation (2.33) becomes

$$2\pi W_p = \frac{\pi i}{2}\int_{-1}^{\infty} K(X)\left[\frac{\partial^2}{\partial X_p^2} + \kappa^2\right] H_0^{(2)}(\kappa|X - X_p|)\, dX, \quad (2.48)$$

as Z_p, $Z \to 0$.

A slight modification to the above form can be achieved by writing

$$\left(\frac{d^2}{d\mu^2} + 1\right) H_0^{(2)}(\mu) = -\frac{1}{\mu}\frac{dH_0^{(2)}}{d\mu} \quad , \tag{2.49}$$

from Bessel's equation (2.34). Also as Z_p, $Z \to 0$,

$$\mu^2 = \kappa^2 (X - X_p)^2 \ ,$$

and

$$2\mu\, d\mu = -2\kappa^2 (X - X_p)\, dX_p \ ,$$

or

$$d\mu = -\frac{\kappa (X - X_p)}{|X - X_p|}\, dX_p \ .$$

Therefore,

$$\frac{dH_0^{(2)}}{d\mu} = \frac{dH_0^{(2)}}{dX_p} \cdot \frac{dX_p}{d\mu} = \frac{dH_0^{(2)}}{dX_p}\left[-\frac{|X - X_p|}{\kappa (X - X_p)}\right] \ , \tag{2.50}$$

$$\frac{d^2 H_0^{(2)}}{d\mu^2} = \frac{d}{d\mu}\left[\frac{dH_0^{(2)}}{dX_p} \cdot \frac{dX_p}{d\mu}\right]$$

$$= \frac{1}{\kappa^2}\frac{d^2 H_0^{(2)}}{dX_p^2} \ . \tag{2.51}$$

Hence, equation (2.49) yields

$$\frac{1}{\kappa^2}\left[\frac{d^2}{dX_p^2} + \kappa^2\right] H_0^{(2)} = \frac{|X - X_p|}{\mu\kappa (X - X_p)} \cdot \frac{dH_0^{(2)}}{dX_p} \ ,$$

or

$$\left[\frac{d^2}{dX_p^2} + \kappa^2\right] H_0^{(2)} = \frac{1}{(X - X_p)} \cdot \frac{dH_0^{(2)}}{dX_p} \ . \tag{2.52}$$

Equation (2.48) thus changes to

$$2\pi W_p = \frac{\pi i}{2} \int_{-1}^{\infty} \frac{K(X)}{(X-X_p)} \cdot \frac{d}{dX_p} H_0^{(2)}(\kappa|X-X_p|)\, dX \tag{2.53}$$

$$= -\frac{\pi i}{2} \int_{-1}^{\infty} \frac{K(X)}{(X-X_p)} H_1^{(2)}(\kappa|X-X_p|)\, dX \tag{2.54}$$

Equations (2.53) and (2.54) are two convenient forms of the two-dimensional, unsteady, compressible flow formulation.

For two-dimensional incompressible flow, both steady and unsteady states, we now refer to equation (2.24) and rewrite

$$2\pi W_p = \int_{-1}^{\infty} \int_{0}^{\infty} K(X,Z) \frac{\partial^2}{\partial Z_p^2} \left(\frac{1}{R}\right) dY\, dX \ , \tag{2.55}$$

where

$$R = \left[(X-X_p)^2 + Y^2 + Z_p^2\right]^{1/2}.$$

Rearranging equation (2.55),

$$2\pi W_p = \int_{-1}^{\infty} K(X,Z) \frac{\partial}{\partial Z_p} \left[\int_{0}^{\infty} \frac{\partial}{\partial Z_p} \left(\frac{1}{R}\right) dY \right] dX \ . \tag{2.56}$$

Consider

$$\frac{\partial}{\partial Z_p}\left(\frac{1}{R}\right) = -\frac{Z_p}{R^3} \ , \tag{2.57}$$

and

$$\int_0^{\infty} \frac{dY}{R^3} = \left[\frac{Y}{\left[(X-X_p)^2+Z_p^2\right]\left[(X-X_p)^2+Y^2+Z_p^2\right]^{1/2}} \right]_0^{\infty}$$

$$= \frac{1}{(X-X_p)^2+Z_p^2} \ . \tag{2.58}$$

Therefore, equation (2.56) becomes,

$$2\pi W_p = -\int_{-1}^{\infty} K(X,Z) \frac{\partial}{\partial Z_p}\left[\frac{Z_p}{(X-X_p)^2+Z_p^2}\right] dX \quad , \qquad (2.59)$$

which reduces to

$$2\pi W_p = \int_{-1}^{\infty} K(X) \frac{\partial}{\partial X}\left(\frac{1}{X-X_p}\right) dX \quad , \qquad (2.60)$$

as Z_p, $Z \to 0$, and noting at

$$\lim_{Z_p \to 0} \frac{\partial}{\partial Z_p}\left[\frac{Z_p}{(X-X_p)^2+Z_p^2}\right] = -\lim_{Z_p \to 0} \frac{\partial}{\partial X}\left[\frac{X-X_p}{(X-X_p)^2+Z_p^2}\right] . \qquad (2.61)$$

Alternatively, equation (2.60) is

$$2\pi W_p = -\int_{-1}^{\infty} \frac{\partial K/\partial X}{X-X_p}\, dX \quad . \qquad (2.62)$$

Three-dimensional incompressible flow, steady and unsteady, formulation is simplified further as follows. From equation (2.24),

$$4\pi W_p = \iint_{\substack{\text{airfoil} + \\ \text{wake}}} K(X,Y,Z) \frac{\partial^2}{\partial Z_p^2}\left(\frac{1}{R}\right) dY\,dX \quad , \qquad (2.63)$$

where

$$R = \left[(X-X_p)^2 + (Y-Y_p)^2 + Z_p^2\right]^{1/2} . \qquad (2.64)$$

As $\nabla_*^2\left(\frac{1}{R}\right) = 0$,

$$\frac{\partial^2}{\partial Z_p^2}\left(\frac{1}{R}\right) = -\left(\frac{\partial^2}{\partial X_p^2} + \frac{\partial^2}{\partial Y_p^2}\right)\left(\frac{1}{R}\right)$$

$$= \frac{\partial}{\partial X}\left[\frac{X-X_p}{R^3}\right] + \frac{\partial}{\partial Y}\left[\frac{Y-Y_p}{R^3}\right] . \qquad (2.65)$$

Therefore, as $Z \to 0$, and for a thin lifting surface at small angles of attach $K(Z_p \to 0)$

$$4\pi W_p = \iint_{\substack{\text{airfoil} \\ \text{wake}}} K(X,Y)\left[\frac{\partial}{\partial X}\left\{\frac{X-X_p}{R^3}\right\} + \frac{\partial}{\partial Y}\left\{\frac{Y-Y_p}{R^3}\right\}\right] dX\,dY. \tag{2.66}$$

Numerical Scheme to Solve Integral Equations

The integrands of the surface integrals appearing in the velocity potential formulations for various types of flows are functions of the unknown discontinuity in the modified velocity potential, K(X,Y), and known functions of the airfoil and wake geometry in the transformed coordinates. These also depend upon the angular frequency of external excitations that are responsible for the unsteady state of the relative flow past the airfoil. In order to facilitate evaluation of K-distribution, the lifting surface is divided into a number of conveniently shaped boxes and the value of K over each box is assumed to be constant. Making use of the wake boundary condition that there can exist no pressure discontinuity in the wake, the value of K at any spanwise location in the wake can be expressed as a function of the value of K at the trailing edge box at the same spanwise location. Hence, the wake is divided into a number of trailing strips and K(X,Y) is considered constant across each strip but to vary with X downstream. When the downwash contributions due to all the boxes and strips are obtained, the problem, in general, is reduced to solving simultaneously a set of as many linear equations as the number of boxes on the lifting surface. Steady and unsteady load

calculations are then carried out in terms of the known doublet distribution and the lifting surface geometry.

Two-Dimensional Incompressible Flow

a. Steady State.

The relation for the downwash at a point X_i on an airfoil is expressed as equation (2.60),

$$2\pi W_i = \int_{\substack{-1 \\ Z\to 0}}^{\infty} K \frac{\partial}{\partial X}\left[\frac{X - X_i}{(X-X_i)^2 + Z^2}\right] dX$$

$$= \int_{-1}^{1} \frac{\partial K/\partial X}{X_i - X}\, dX = \frac{K_{te}}{X_i - 1} - \int_{-1}^{1} K \frac{\partial}{\partial X}\left(\frac{1}{X_i - X}\right) dX \quad (3.1)$$

$$= \frac{K_{te}}{X_i - 1} + \sum_{j=1}^{N} K_j \left[\frac{1}{X_i - X_j + D} - \frac{1}{X_i - X_j - D}\right].$$

The airfoil is divided into N equal strips of width 2D and K is assumed to be a constant over each strip. K_{te} is related to K_N and is normally taken as equal to K_N. Equation (3.1) can be written as

$$2\pi \{W\} = [A]\{K\} \quad , \quad (3.2)$$

where

$$a_{ij} = \frac{1}{X_i - X_j + D} - \frac{1}{X_i - X_j - D} \quad , \quad j \neq N$$

and

$$= \frac{1}{X_i - 1 + 2D} \quad , \quad j = N .$$

For a prescribed boundary condition, W_i is known. This is a non-dimensional downwash velocity at a point X_i. For a constant angle of attack case, $W_i = \alpha (i = 1, 2, \ldots, N)$ and the lift per unit span is

$$L' = \rho U k_{te} = \rho U^2 \ell K_{te} = \rho U^2 \ell K_N$$

or

$$C_\ell = L'/(\rho U^2 \ell) = K_N \quad . \tag{3.3}$$

Pitching moment per unit span about the mid-chord axis is (nose-up positive)

$$M' = \rho U^2 \ell^2 \int_{-1}^{1} \frac{\partial K}{\partial X} X \, dX$$

or

$$C_m = M'/(\rho U^2 \ell^2) = K_N - 2D \sum_{n=1}^{N} K_n \tag{3.4}$$

The analytical solution for K distribution is given by

$$K = 2(\theta + \sin\theta)\alpha \tag{3.5}$$

where $\theta = \cos^{-1}(-X)$

The computer program based upon the constant K distribution over each strip is very simple, especially when the collocation points of each strip are taken at the center of each strip. For this case, the results are presented below for several values of N and are compared with the exact results.

	Exact Solution	Lifting Surface Solutions N=5	N=20	N=30
$C_{\ell\alpha}$	6.2832	6.2831	6.2829	6.2818
$C_{m\alpha}$	-3.1416	-2.6431	-2.9885	-3.0384

The computational time on AMDAHL 470 for all three cases (N=5, 20, and 30) was less than 0.54 seconds using WATFIV compiler which is only 1/5 th as fast as FORTRAN G or H compiler. As can be seen, the results for the coefficients are in excellent agreement indicating that the computed K_N is close to the exact value even for N=5 case. The moment coefficient continues to reach the exact value as N is increased. The K distribution is plotted in Fig. 1 and it can be seen, it is substantially different from the exact distribution, especially near the leading edge region. To improve this situation the collocation point of the leading edge strip is varied from 1D to 0.75D from the leading edge and the results of $K(K/2\pi\alpha)$ are presented below for a 5 strip model.

			$K/2\pi\alpha$		
X=	-0.8	-0.4	0	0.4	0.8
Exact	0.396	0.661	0.818	0.923	0.986
1.00D	0.492	0.711	0.852	0.945	1.000
0.95D	0.468	0.697	0.840	0.935	0.990
0.90D	0.443	0.684	0.829	0.925	0.980
0.85D	0.418	0.670	0.818	0.914	0.970
0.80D	0.394	0.656	0.806	0.904	0.960
0.75D	0.369	0.643	0.795	0.893	0.950

As can be seen from the above Table, the K distribution has improved towards the leading edge as the collocation point location is moved toward the leading edge; however, the trailing edge values are in error for this collocation point location, resulting in a decrease in the lift coefficient. Another scheme is tried to correct this situation. In addition to the leading edge strip collocation point variation, the trailing edge value,

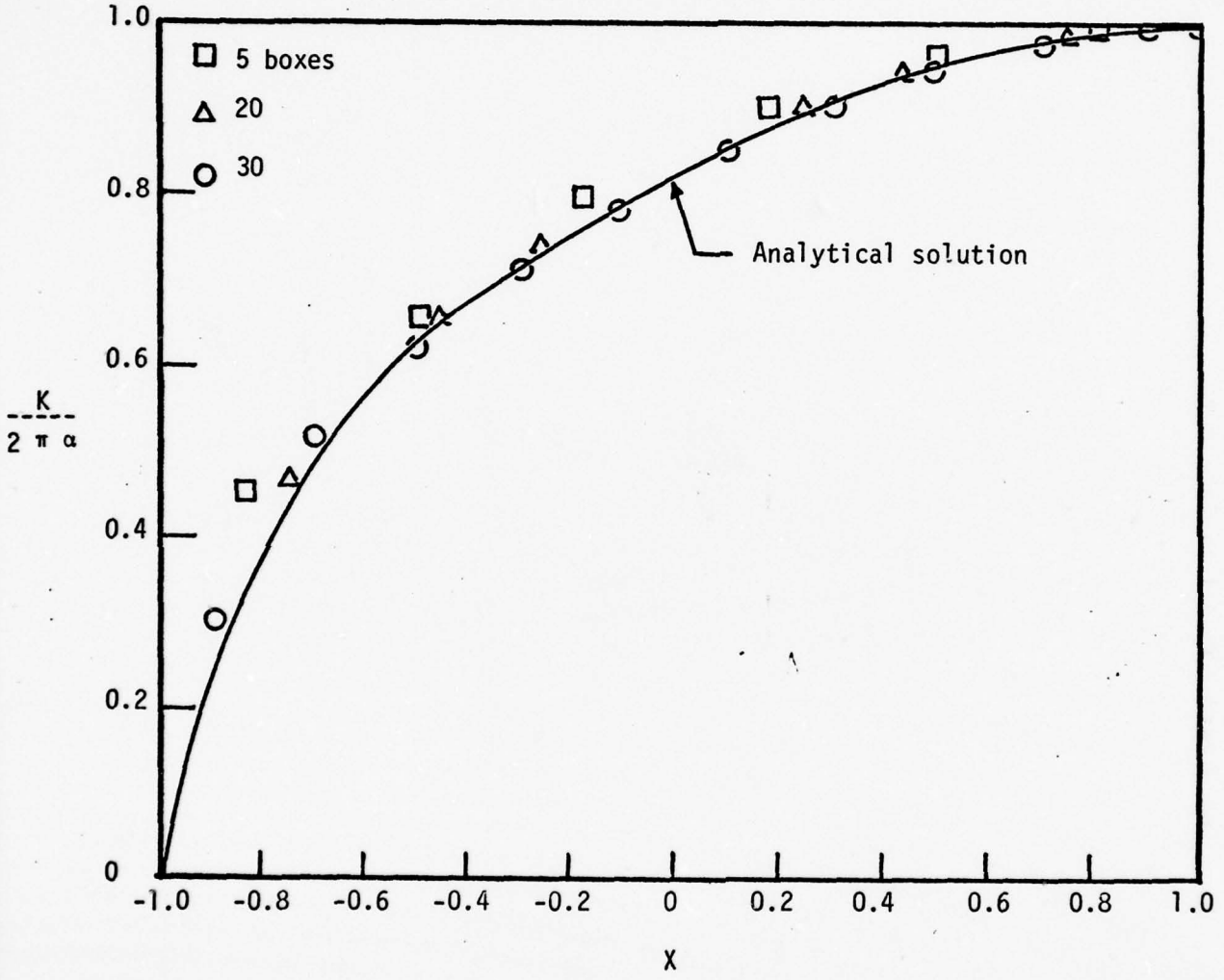

FIGURE 1. Comparison of the Present Method with Analytical Solution

K_{te}, is expressed by the relation

$$K_{te} = \frac{9K_N - K_{N-1}}{8}$$

in place of $K_{te} = K_N$, and the results are tabulated below.

	$K/2\pi\alpha$				
X =	-0.8	-0.4	0	0.4	0.8
Exact	0.396	0.661	0.818	0.923	0.986
1.00D	0.499	0.722	0.866	0.964	1.023
0.96D	0.480	0.711	0.857	0.955	1.015
0.92D	0.460	0.700	0.843	0.947	1.007
0.88D	0.440	0.689	0.839	0.939	0.998
0.84D	0.420	0.678	0.830	0.931	0.990
0.80D	0.400	0.667	0.821	0.922	0.982

As can be seen from the above table for the collocation point location at 0.800D and the modified trailing edge relation resulted in an excellent agreement with the exact result. In a recent paper, Kocurek and Tangler[53] discussed a systematic means of the collocation point selection.

b. Unsteady State.

In the case of unsteady flow, a periodic motion is assumed and the doublet distribution is assumed to be $K'\exp(ipt) = K'\exp(i\omega T)$. The relation for the downwash (amplitude) at a point X_i on an airfoil is expressed as equation (2.62)

$$2\pi W_i' = \int_{-1}^{\infty} \frac{\partial K'/\partial X}{X_i - X}\, dX$$

$$= \frac{K'_{te}}{X_i - 1} - \int_{-1}^{1} K' \frac{\partial}{\partial X}\left(\frac{1}{X_i - X}\right) dX + \int_{1}^{\infty} \frac{\partial K'/\partial X}{X_i - X}\, dX \quad (3.6)$$

The boundary condition in the wake and at the trailing edge is expressed as

$$i\omega K' + \frac{\partial K'}{\partial X} = 0 \quad , \quad X \geqslant 1 \quad , \tag{3.7}$$

and K' in the wake can be expressed in terms of K'_{te} by solving equation (3.7),

$$K'_{wake} = K'_{te}\, e^{-i\omega(X-1)} \tag{3.8}$$

The airfoil is divided into N equal strips and K' is assumed to be a constant over each strip. Equations (3.6) and (3.8) are combined to yield

$$2\pi W_i' = i\omega K'_{te} \int_1^{\infty} \frac{e^{-i\omega(X-1)}}{X - X_i}\, dX + \frac{K'_{te}}{X_i - 1} + \sum_{j=1}^{N} K'_j \left[\frac{1}{X_i - X_j + D} - \frac{1}{X_i - X_j - D} \right] \tag{3.9}$$

Making use of the wake boundary condition at the trailing edge several possible relations can be obtained for K'_{te} in terms of K'_N. One such frequently used relation is

$$K'_{te} = F K'_N \quad , \tag{3.10}$$

where

$$F = 1/\left[e^{-i\omega D} + 2i\omega D \right] .$$

Equations (3.9) and (3.10) are combined to yield

$$2\pi \{W\} = [A]\{K\} \quad ,$$

where

$$a_{ij} = \frac{1}{X_i - X_j + D} - \frac{1}{X_i - X_j - D} \quad , \quad j \neq N$$

and

$$a_{ij} = \frac{1}{X_i - X_j + D} - \frac{1}{X_i - X_j - D} + \frac{F}{X_i - 1} + i\omega F \int_1^{\infty} \frac{e^{-i\omega(X-1)}}{X - X_i}\, dX \quad , \quad j = N$$

The infinite integrals in the term a_{iN} are evaluated by separating into real and imaginary parts. These terms are expressed in terms of infinite series and are analytically integrated. The relation is given by

$$\int_1^\infty \frac{e^{-i\omega(X-1)}}{X-X_i}\,dX = e^{i\omega(1-X_i)}\left[\left\{-\gamma-\ln\omega(1-X_i) + \frac{\omega^2(1-X_i)^2}{2\cdot 2!} - \frac{\omega^4(1-X_i)^4}{4\cdot 4!}+\cdots\right\} - i\left\{\frac{\pi}{2}-\omega(1-X_i)+\frac{\omega^3(1-X_i)^3}{3\cdot 3!}-\cdots\right\}\right] \tag{3.12}$$

The above developed formulation is equally valid for oscillating airfoils as is for oscillatory flows (like gust). The boundary conditions are usually prescribed in either case. For airfoils undergoing flapping and pitching oscillations (about the mid-chord) the boundary condition is

$$W_i' = i\omega Z' + (1 + i\omega X_i)\alpha', \tag{3.13}$$

and for oscillatory flow

$$W_i' = \alpha' e^{-i\omega X_i}, \tag{3.14}$$

where Z' and α' are the flapping and hitching amplitudes, respectively.

The unsteady lift and moment coefficients are then expressed as

$$\left.\begin{aligned} \frac{L'}{\rho U^2 \ell} &= C_{\ell z} Z + C_{\ell\alpha}\alpha, \\ \text{and}\quad \frac{M'}{\rho U^2 \ell^2} &= C_{mz} Z + C_{m\alpha}\alpha, \end{aligned}\right\} \tag{3.15}$$

where

$$\left.\begin{aligned} C_{\ell(\cdot)} &= K_{te(\cdot)} + i\omega 2D \sum_{j=1}^{N} K_{j(\cdot)}, \\ \text{and} \\ C_{m(\cdot)} &= -K_{te(\cdot)} + 2D \sum_{j=1}^{N} K_{j(\cdot)} - i\omega 2D \sum_{j=1}^{N} K_j X_j \end{aligned}\right\} \quad (3.16)$$

The parentheses, ( ), in equation (3.16) can be replaced either by Z or α and the appropriate boundary conditions are applied.

The analytical expressions for oscillating airfoils are

$$\left.\begin{aligned} C_{\ell z} &= 2\pi\left(C + \frac{i\omega}{2}\right) i\omega, \\ C_{\ell\alpha} &= 2\pi\left[C\left(1 + \frac{i\omega}{2}\right) + \frac{i\omega}{2}\right], \\ C_{mz} &= i\omega\pi C \\ \text{and} \\ C_{m\alpha} &= \pi\left[C\left(1 + \frac{i\omega}{2}\right) - \frac{i\omega}{2}\left(1 + \frac{i\omega}{4}\right)\right], \end{aligned}\right\} \quad (3.17)$$

and for the gust flow,

$$C_{\ell\alpha} = 2\pi\left[C\left\{J_0(\omega) - i J_1(\omega)\right\} + i J_1(\omega)\right], \quad (3.18)$$

where

$$C = \frac{H_1^{(2)}(\omega)}{H_1^{(2)}(\omega) + i H_0^{(2)}(\omega)}$$

$$H_1^{(2)} = J_1 - i Y_1$$

and

$$H_0^{(2)} = J_0 - i Y_0$$

For collocation points located at the centers of each strip results are presented below for both cases along with the comparison with the exact results

Oscillating Airfoils

ω	N	$C_{\ell z}$	$C_{\ell\alpha}$	C_{mz}	$C_{m\alpha}$
0.1	exact	0.077+0.523i	5.281-0.507i	0.054+0.261i	2.645-0.568i
0.1	10	0.074+0.525i	5.296-0.500i	0.056+0.279i	2.828-0.588i
0.1	20	0.074+0.524i	5.293-0.493i	0.055+0.272i	2.750-0.582i
0.1	30	0.075+0.524i	5.291-0.493i	0.055+0.269i	2.718-0.579i
0.2	exact	0.111+0.914i	4.690-0.100i	0.119+0.457i	2.361-0.678i
0.2	10	0.103+0.922i	4.718-0.102i	0.122+0.490i	2.524-0.689i
0.2	20	0.104+0.920i	4.713-0.085i	0.121+0.476i	2.454-0.692i
0.2	30	0.105+0.919i	4.710-0.083i	0.121+0.470i	2.426-0.690i
0.3	exact	0.055+1.253i	4.347+0.443i	0.169+0.627i	2.209-0.721i
0.3	10	0.043+1.269i	4.386+0.428i	0.170+0.672i	2.360-0.718i
0.3	20	0.044+1.265i	4.378+0.456i	0.172+0.652i	2.294-0.730i
0.3	30	0.045+1.263i	4.374+0.459i	0.172+0.644i	2.269-0.731i
0.4	exact	-0.088+1.571i	4.134+1.005i	0.207+0.785i	2.130-0.754i
0.4	10	-0.105+1.595i	4.183+0.979i	0.204+0.842i	2.271-0.735i
0.4	20	-0.104+1.590i	4.173+1.015i	0.210+0.816i	2.210-0.757i
0.4	30	-0.102+1.587i	4.167+1.022i	0.211+0.807i	2.186-0.761i
0.5	exact	-0.312+1.879i	3.994+1.563i	0.237+0.939i	2.095-0.789i
0.5	10	-0.332+1.912i	4.053+1.525i	0.225+1.006i	2.230-0.753i
0.5	20	-0.333+1.905i	4.039+1.570i	0.237+0.975i	2.171-0.785i
0.5	30	-0.330+1.900i	4.031+1.579i	0.239+0.964i	2.148-0.793i

Evaluation of the above listed results indicate that the numerical solution is reasonably accurate even for 10 strip case. The computer program is very efficient and the computational time for all 15 cases (5 ω's and 3 N's) was 4.58 seconds using WATFIV compiler. For oscillatory flow the numerical results along with the comparison with the analytical results are illustrated below.

Oscillatory Flow

ω	N	$C_{\ell\alpha/2\pi}$
1	exact	0.3687+0.1259i
1	5	0.3868+0.1553i
1	9	0.3838+0.1457i
1	15	0.3812+0.1394i
1	25	0.3790+0.1349i
2	exact	0.0816+0.2680i
2	5	0.0707+0.2840i
2	9	0.0789+0.2712i
2	15	0.0823+0.2677i
2	25	0.0840+0.2664i
3	exact	-0.1452+0.1778i
3	5	-0.1705+0.1587i
3	9	-0.1623+0.1513i
3	15	-0.1562+0.1559i
3	25	-0.1521+0.1613i
4	exact	-0.1980-0.0207i
4	5	-0.1932-0.0948i
4	9	-0.2053-0.0655i
4	15	-0.2062-0.0509i
4	25	-0.2051-0.0410i
5	exact	-0.0812-0.1586i
5	5	-0.0415-0.2783i
5	9	-0.0645-0.1919i
5	15	-0.0746-0.1725i
5	25	-0.0794-0.1650i

The values presented in the above Table are for very high reduced frequencies which are of considerable importance in acoustics. Also based on the results, one can conclude that the numerical lifting surface technique yields a reasonable solution if at least 15 strips are considered. Several other schemes were attempted varying the leading edge strip collocation point location. These schemes improved the results but however, the collocation point location was found to be a strong function of reduced frequency and this also increased the computational time due to the lack of symmetry.

Two-Dimensional Compressible Flow

The relation between the downwash at any point X_i on a thin airfoil in subsonic flow and the doublet distribution is derived in Chapter II, equation (2.48) It is expressed as

$$2\pi W_i = \frac{\pi i}{2}\int_{-1}^{\infty} K(X)\left[\frac{\partial^2}{\partial X^2} + \kappa^2\right] H_0^{(2)}(\kappa|X-X_p|)\,dX. \quad (3.19)$$

The wake boundary condition is

$$i\nu K' + \frac{dK'}{dX} = 0 \quad , \quad X \geq 1 \ , \quad (3.20)$$

from which K′ in the wake can be expressed in terms of K'_{te}. The relation is

$$K'_{wake} = K'_{te}\, e^{-i\nu(X-1)} \ , \quad X \geq 1 \ . \quad (3.21)$$

Equations (3.19) and (3.21) are combined to yield

$$2\pi W'_i = \frac{\pi i}{2}\left[\int_{-1}^{1} K'\left(\frac{\partial^2}{\partial X^2} + \kappa^2\right)\Psi\, dX + K'_{te}\int_{1}^{\infty} e^{-i\nu(X-1)}\left(\frac{\partial^2}{\partial X^2} + \kappa^2\right)\Psi\, dX\right], \quad (3.22)$$

where

$$\Psi(\bar{X}) = H_0^{(2)}(\kappa|X-X_i|) \ , \ \bar{X} = \kappa|X-X_i| \ .$$

The airfoil is divided into N equal strips of width, 2D, and K is assumed to be a constant over each strip. Equation (3.22) is then reduced to

$$2\pi W'_i = \frac{\pi i}{2}\left[\sum_{j=1}^{N} K'_j\left\{\left.\frac{\partial\Psi}{\partial X}\right|_{\bar{X}_j-D}^{\bar{X}_j+D} + \frac{\kappa^2 D}{3}\left(\Psi(\bar{X}_j+D) + 4\Psi(\bar{X}_j) + \Psi(\bar{X}_j-D)\right)\right\} - K'_{te}\left\{\left.\frac{\partial\Psi}{\partial X}\right|_{\bar{X}_{te}} + i\nu\Psi(\bar{X}_{te}) + \omega\nu\int_{1}^{\infty} e^{-i\nu(X-1)}\Psi(\bar{X})\,dX^{te}\right\}\right]. \quad (3.23)$$

The wake boundary condition is used to express K'_{te} in terms of K'_N and the relation is

$$K'_{te} = FK'_N = K_N / [e^{-i\nu D} + 2i\nu D] \quad . \tag{3.24}$$

Equations (3.23) and (3.24) are combined to yield a set of N simultaneous equations, i=1, 2, ..., N. The Hankel function has a singularity when its argument is zero. The evaluation of the derivative of Ψ presents no problem since the point of evaluation is, at the least, separated from the collocation point by D. The derivative of the Hankel function is

$$\frac{\partial \Psi}{\partial X} = \kappa \frac{(X_i - X)}{|X - X_i|} H_1^{(2)}(\kappa |X - X_i|) \quad . \tag{3.25}$$

The second term in equation (3.23) is obtained by using Simpson's 1/3 rule and it poses a problem since the $\Psi(X_j)$ term becomes infinite when X_j is at the collocation point, X_i. This situation is alleviated by using the Struve's function. At the singularity point, the portion of the surface being integrated over is

$$\int_{X_j - D}^{X_j + D} \Psi(\kappa |X - X_j|)\, dX = \frac{2}{\kappa} \int_0^{\kappa D} H_0^{(2)}(\bar{X}')\, d\bar{X}'$$

$$= 2D H_0^{(2)}(D') + \pi D \left[H_1^{(2)}(D') \bar{H}_0(D') - H_0^{(2)}(D') \bar{H}_1(D') \right], \tag{3.26}$$

where

$$D' = \kappa D$$

$$\bar{H}_0(D') = \frac{2}{\pi} \left(D' - \frac{D'^3}{3^2} + \frac{D'^5}{3^2 \cdot 5^2} - \cdots \right) ,$$

and

$$\bar{H}_1(D') = \frac{2}{\pi} \left(\frac{D'^2}{3} - \frac{D'^4}{3^2 \cdot 5} + \frac{D'^6}{3^2 \cdot 5^2 \cdot 7} - \cdots \right) .$$

The wake integration involving an infinite integration is simplified and is expressed in the form

$$\int_1^{\infty} e^{-i\nu(X-1)} H_0^{(2)}(K|X-X_i|)\,dX = -e^{i\nu(1-X_i)}\left[\frac{2}{\nu\pi\beta}\ln\left(\frac{1-\beta}{M}\right) + \int_0^{1-X_i} e^{-i\nu X'} H_0^{(2)}(K|X'|)\,dX'\right] . \tag{3.27}$$

Equations (3.24) - (3.27) are incorporated in equation (3.23) and the result is that the problem reduces to a set of simultaneous equations which can be solved for a given set of boundary conditions.

Boundary Conditions

$$W = \frac{d\Phi}{dZ} = \frac{1}{U\beta}\frac{d\phi}{dz} e^{-i(\lambda X + \omega T)} , \tag{3.28}$$

where

$$\frac{d\phi}{dz} = w = \frac{d\zeta}{dt} ,$$

and ζ is the vertical displacement.

For an airfoil undergoing flapping and pitching oscillations about mid-chord position

$$\zeta = z' e^{i\omega T} + \alpha' x e^{i\omega T} . \tag{3.29}$$

Equations (3.28) and (3.29) are combined to yield

$$W = \left[i\omega Z' + (1 + i\omega X)\alpha'\right]\frac{e^{-i\lambda X}}{\beta} , \tag{3.30}$$

where Z' and α' are the amplitudes in flapping and pitching motions, respectively.

For oscillatory (gust) flow

$$\zeta = \alpha' e^{i(\omega T - \omega X)} \tag{3.31}$$

Equations (3.28) and (3.31) are combined to yield

$$W = \alpha' e^{-i\omega X} e^{-i\lambda X/\beta} = \alpha' e^{-i\nu X/\beta} . \tag{3.32}$$

Lift and Moment Coefficients

$$k = \phi_u - \phi_\ell = U\ell K e^{i(\lambda X + \omega T)} , \tag{3.33}$$

and

$$\frac{\partial k}{\partial t} + U\frac{\partial k}{\partial x} = \frac{1}{\rho}\tilde{\ell}(x) , \tag{3.34}$$

where $\tilde{\ell}(x)$ is the pressure difference.

Equations (3.33) and (3.34) are combined to yield

$$\tilde{\ell}'(x) = \rho U^2\left(\frac{\partial \bar{K}}{\partial X} + i\omega\bar{K}\right) , \tag{3.35}$$

where $\bar{K} = K e^{i\lambda X}$

Then the lift and moment coefficients are evaluated using equations (3.15) and (3.16), respectively. Some results and computational times are presented below in tabular form for both cases of oscillating airfoils and oscillatory flows.

Oscillating Airfoils

ω	M	$C_{\ell z}$	$C_{\ell\alpha}$	C_{mz}	$C_{m\alpha}$
0.1	0.01	0.073+0.525i	5.297-0.491i	0.058+0.286i	2.888-0.602i
0.1	0.50	0.116+0.569i	5.760-0.901i	0.088+0.307i	3.114-0.923i
0.1	0.60	0.141+0.591i	5.996-1.144i	0.107+0.316i	3.219-1.121i
0.1	0.70	0.179+0.618i	6.296-1.519i	0.136+0.326i	3.332-1.433i
0.1	0.80	0.242+0.650i	6.652-2.144i	0.184+0.330i	3.392-1.967i
0.2	0.01	0.102+0.924i	4.730-0.088i	0.125+0.501i	2.582-0.709i
0.2	0.50	0.183+0.977i	5.050-0.483i	0.193+0.517i	2.695-1.099i
0.2	0.60	0.225+0.998i	5.189-0.690i	0.231+0.519i	2.718-1.323i
0.2	0.70	0.288+1.025i	5.372-1.008i	0.288+0.512i	2.706-1.669i
0.2	0.80	0.384+1.046i	5.550-1.522i	0.373+0.473i	2.519-2.224i
0.3	0.01	0.040+1.277i	4.416+0.447i	0.176+0.690i	2.422-0.741i
0.3	0.50	0.154+1.340i	4.721+0.073i	0.286+0.695i	2.488-1.197i
0.3	0.60	0.214+1.371i	4.879-0.135i	0.347+0.687i	2.485-1.464i
0.3	0.70	0.302+1.403i	5.061-0.454i	0.435+0.655i	2.396-1.869i
0.3	0.80	0.444+1.418i	5.218-1.020i	0.554+0.548i	1.996-2.484i
0.4	0.01	-0.112+1.601i	4.201+1.009i	0.210+0.862i	2.325-0.757i
0.4	0.50	0.041+1.704i	4.602+0.626i	0.374+0.862i	2.394-1.299i
0.4	0.60	0.125+1.751i	4.802+0.399i	0.465+0.841i	2.366-1.623i
0.4	0.70	0.254+1.798i	5.032+0.016i	0.592+0.773i	2.196-2.112i
0.4	0.80	0.468+1.794i	5.149-0.700i	0.726+0.563i	1.522-2.747i
0.5	0.01	-0.345+1.924i	4.081+1.564i	0.233+1.033i	2.288-0.775i
0.5	0.50	-0.142+2.089i	4.619+1.155i	0.465+1.028i	2.367-1.423i
0.5	0.60	-0.025+2.160i	4.876+0.883i	0.593+0.986i	2.306-1.817i
0.5	0.70	0.171+2.226i	5.164+0.383i	0.765+0.861i	2.021-2.399i
0.5	0.80	0.477+2.170i	5.160-0.535i	0.870+0.523i	1.030-2.937i

The computational time for all the above 25 cases was 4.39 seconds using FORTRAN G Compiler. In this case, the airfoil is divided into 11 strips.

Oscillatory Flow

ω	M	$C_{\ell\alpha}$	$C_{m\alpha}$
0.10	0.01	5.188-0.967i	2.812-0.549i
0.10	0.50	5.597-1.410i	3.007-0.838i
0.10	0.60	5.800-1.668i	3.093-1.010i
0.10	0.70	6.049-2.057i	3.177-1.277i
0.10	0.80	6.319-2.682i	3.196-1.711i
0.50	0.01	3.391-0.159i	1.794-0.142i
0.50	0.50	3.520-0.526i	1.716-0.408i
0.50	0.60	3.554-0.711i	1.629-0.526i
0.50	0.70	3.545-0.973i	1.441-0.643i
0.50	0.80	3.367-1.280i	1.095-0.576i
1.00	0.01	2.404+0.924i	1.226+0.451i
1.00	0.50	2.736+0.459i	1.126+0.166i
1.00	0.60	2.742+0.183i	0.974+0.102i
1.00	0.70	2.568-0.064i	0.784+0.200i
1.00	0.80	2.462-0.110i	0.841+0.354i

The computational time for all of the above 15 cases, taking 11 strips over the airfoil, was 4.09 seconds.

The present lifting surface method resulted in the development of a very efficient computer program for a 2-dimensional compressible flow case, which in general has one of the most complicated formulations.

i) Steady State Application to Marine Propellers

Elchuri[54] applied the velocity potential formulation and the associated numerical technique to the problem of estimating the steady and unsteady loading distribution on typical ship propellers. In order to study the response of the method, two B series propellers, B-3.35 and B-3.50, were examined. Expanded outlines of these two types of blades are shown in Figs. 2 and 3. As a first approximation, blades were treated as thin lifting surfaces with no wake. The lifting surface was divided into a grid of 100 boxes with ten such boxes along each chord at an equal number of spanwise locations. To obtain the distribution of the discontinuity in the velocity potential on the blade surface, the presence of all the blades and their wakes was considered. The doublet distribution obtained as a result of solving a set of simultaneous equations as d scussed earlier is related to the differential pressure distribution on the blade at any point P as

$$p_f - p_b = \rho \vec{w}_\infty \cdot \nabla k \quad ,$$

where the relative free stream velocity is

$$\vec{w}_\infty = \vec{v}_\infty + \Omega y \hat{i} - \Omega x \hat{j} + v_a \hat{k} \quad .$$

The thurst produced by a blade section at a mean radius r_m is the component of the resultant of lift and drag forces along the direction of propeller advance. Therefore, per unit span,

$$\vec{T} = \sum_{r_m \text{ const.}} [(\vec{L} + \vec{D}) \cdot \hat{k}] \hat{k} \quad ,$$

where the lift per unit span due to a box with P as the collocation point is

$$\vec{L} = \vec{\lambda} \int_1^2 (p_f - p_b) ds$$

$$= \left. \frac{\vec{n} - (\vec{n} \cdot \vec{s}) \vec{s}}{|\vec{n} - (\vec{n} \cdot \vec{s}) \vec{s}|} \right|_P \rho \left[w_{\infty_2} k_2 - w_{\infty_1} k_1 - \int_1^2 k \frac{dw_\infty}{ds} ds \right] ,$$

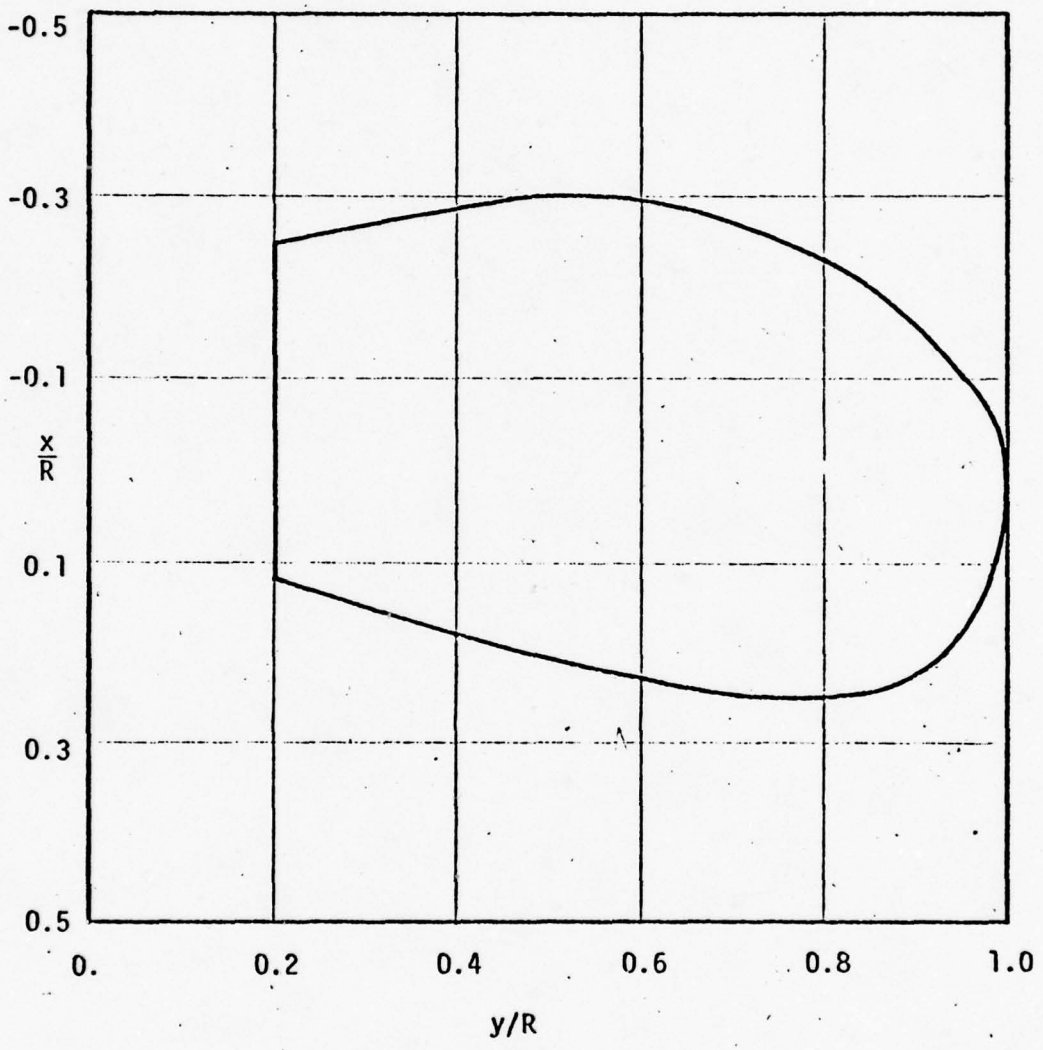

Figure 2. Expanded Outline, B-3.35 Marine Propeller

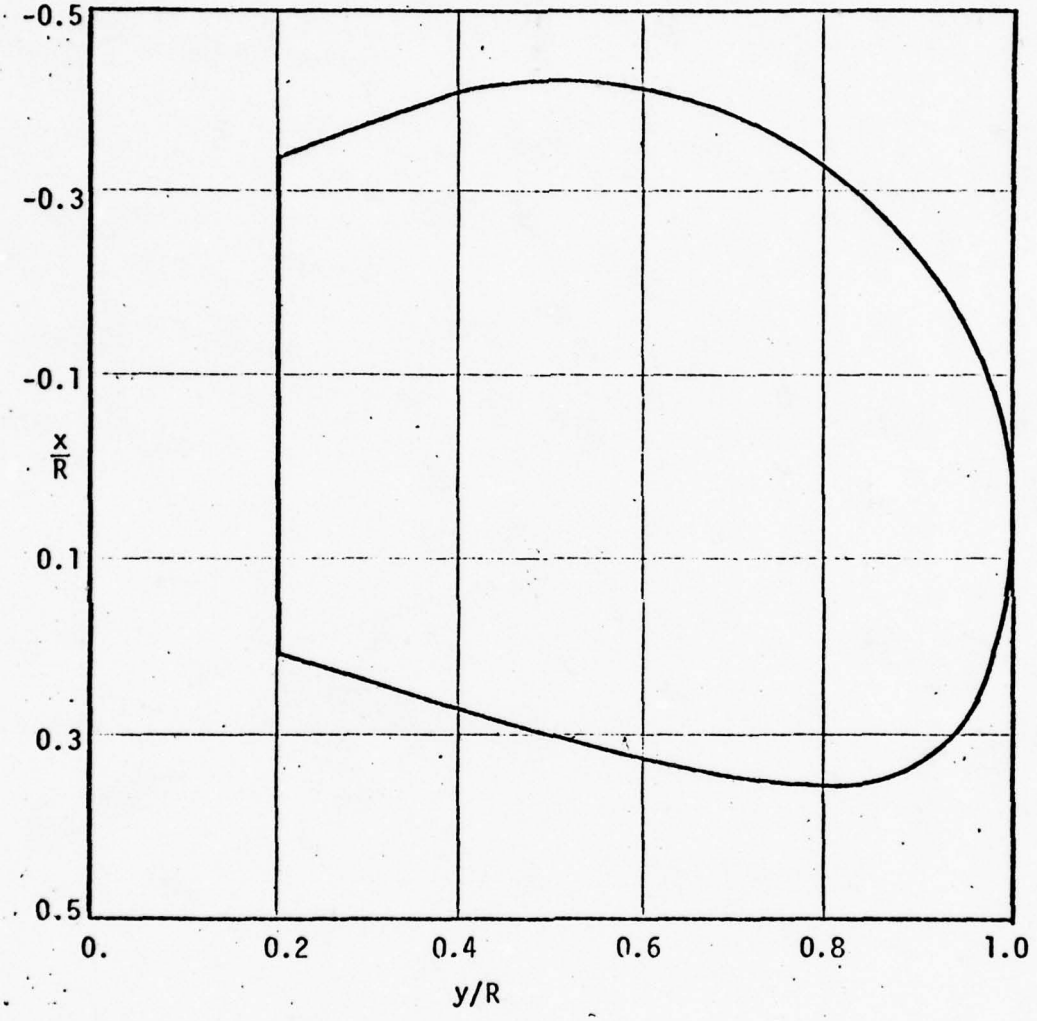

Figure 3. Expanded Outline, B-3.50 Marine Propeller

and the profile drag per unit span at P is

$$\vec{D} = \vec{s}\, C_D \left(\tfrac{1}{2}\rho w_\infty^2 \ell\right) ,$$

with the local drag coefficient C_D generally stated as an empirical function of the angle of attack.

Torque necessary to overcome water resistance per unit span to turn the propeller at a constant angular velocity Ω is

$$\vec{Q} = \sum_{r_M \text{ const.}} \left[\{-\vec{r}_{p/o} \times (\vec{L} + \vec{D})\} \cdot \hat{k}\right] \hat{k} ,$$

where $\vec{r}_{p/o}$ is the position vector of point P with reference to origin O.

It is customary to describe the propeller characteristics in terms of thrust and torque coefficients (aggregated over the entire span), and the propeller efficiency, as functions of the advance coefficient J. These parameters are defined as,

$$\left.\begin{aligned} &\text{Thrust coefficient,} \quad K_T = \Sigma T/(\rho N^2 D^4) \\ &\text{Torque coefficient,} \quad K_Q = \Sigma Q/(\rho N^2 D^5) \\ &\text{Propeller efficiency,} \quad \eta = \frac{\Sigma T \cdot V_a}{\Sigma Q (2\pi N)} = \frac{K_T J}{2\pi K_Q} \end{aligned}\right\}$$

where the advance coefficient is

$$J = V_a/(ND) .$$

Thrust and orque coefficients together with propeller efficiency as functions of the advance coefficient at a pitch to diameter ratio of 1.0 for B-3.35 and B-3.50 marine propellers are shown in Figs. 4 and 5. A good comparison with the experimental results of reference 54 reflect upon the feasibility of the present lifting surface method with regard to its applicability to marine propellers.

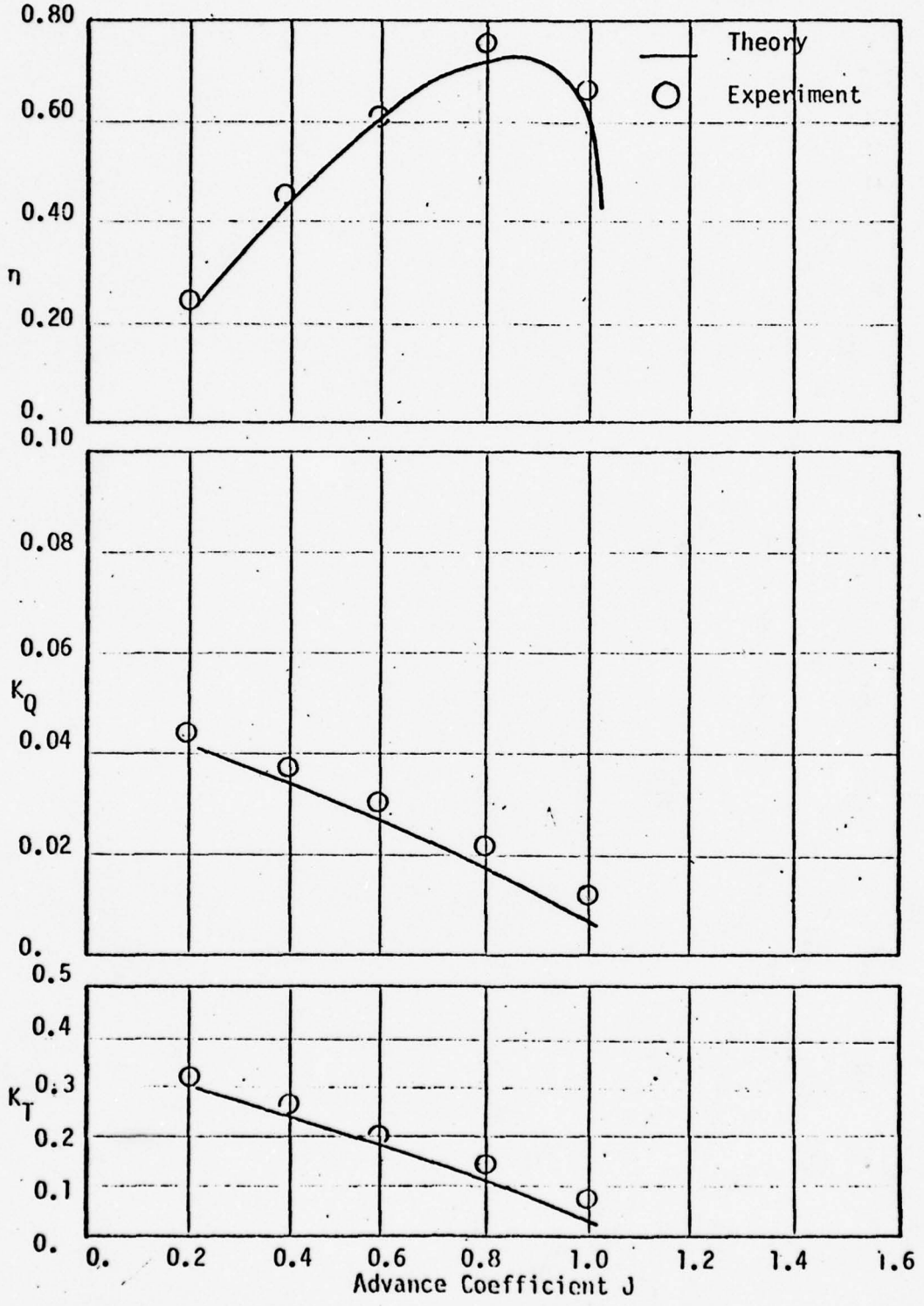

Figure 4. B-3.35 Characteristics P/D = 1.0

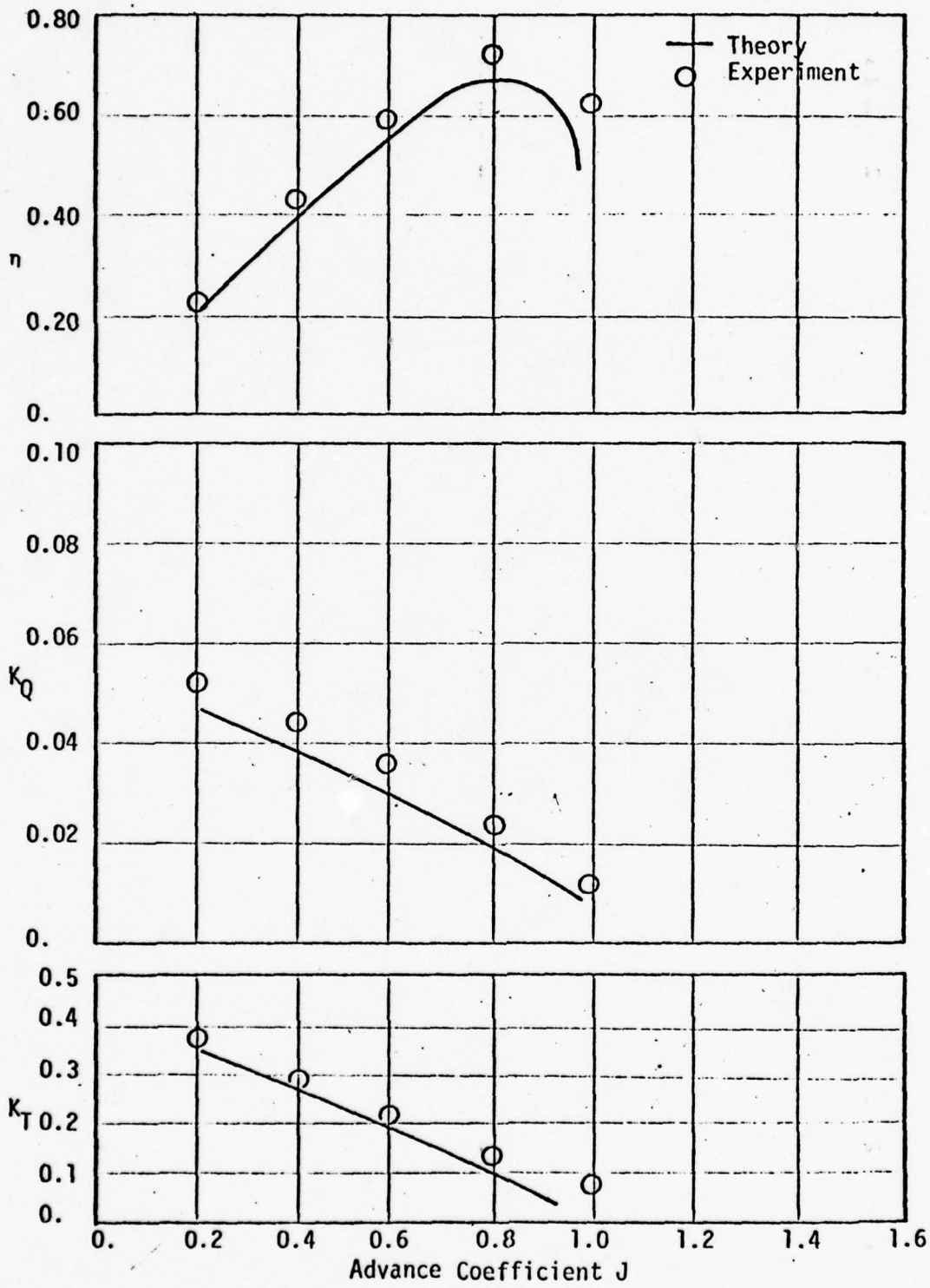

Figure 5. B-3.50 Characteristics P/D = 1.0

ii) Analysis of Unsteady Airloads of Helicopter Rotors in Hover

Schatzle[55] applied the present numerical lifting method to predict the unsteady airloads on a multi-bladed helicopter rotor in hover using a realistic wake representation. The method employed a velocity potential formulation and the wake geometry was prescribed using Landgrebe's model. A summary of the results were presented at the AIAA 15th Aerospace Sciences Meeting (Ref. 56, also to be published in the Journal of Aircraft). A brief discussion of the method and the results are presented in this section.

Basic Equations and Numerical Method

The relation between the downwash velocity at a point on a rotor blade (wing) and distribution of doublets over the blade and wake surfaces is derived in a previous section (Eq. 2.23) and is given by

$$4\pi W_p = \iint_{\substack{\text{wing} \\ + \\ \text{wake}}} K \frac{\partial^2}{\partial z^2}\left(\frac{e^{-ikR}}{R}\right) dS \qquad (4.1)$$

where K, the local doublet intensity, is equal to the discontinuity in the transformed potential across the wing or wake. The value of K at a point in the wake may be determined from the value of K at the trailing edge of the wing in the following manner. From Euler's equation, the local pressure difference across a thin surface is related to the corresponding discontinuity in

potential by

$$\tilde{\ell} = \rho U^2 \left(i\nu K + \frac{\partial K}{\partial x} \right) e^{i(\lambda x + \omega T)} \quad (4.2)$$

Since the wake cannot support a pressure discontinuity, =0 in eq. (4.2) and thus,

$$K(x,Y) = K(x_{te},Y)\, e^{-i\nu(x-x_{te})} \quad (4.3)$$

$$4\pi W_p = \iint_{wing} K \frac{\partial^2}{\partial z^2} \left(\frac{e^{-i\lambda R}}{R} \right) dS + \iint_{wake} K_{te}\, e^{-i\nu(x-x_{te})} \frac{\partial^2}{\partial z^2} \left(\frac{e^{-i\lambda R}}{R} \right) dS. \quad (4.4)$$

In the numerical technique developed, it is assumed that there are M panels along the chord of the blade and N panels along the span. For a panel mn the local doublet intensity, K_{mn}, is constant over the panel and may therefore be removed from the integration of eq. (4.4) over that panel. Similarly, $K_{te,n}$ may be expressed as K_{Mn} and removed from the integration of eq. (4.4) over that strip. If the integrations in eq. (4.4) are carried out over each panel and strip and then combined to

form the entire surface integration, eq. (4.4) may be written in influence coefficient form as

$$4\pi W_p = \sum_{m=1}^{M}\sum_{n=1}^{N} A_{p,mn} K_{mn} + \sum_{n=1}^{N} B_{p,n} K_{Mn}, \quad (4.5)$$

where

$$A_{p,mn} = \iint_{Panel_{mn}} \frac{\partial^2}{\partial z^2}\left(\frac{e^{-ikR}}{R}\right) dS_{mn} \quad (4.5a)$$

and

$$B_{p,n} = \iint_{strip\,n} e^{-ik(x-x_{te})} \frac{\partial^2}{\partial z^2}\left(\frac{e^{-ikR}}{R}\right) dS_n \quad (4.5b)$$

Here $A_{p,mn}$ represents the downwash velocity induced at P due to a unit velocity doublet at the panel mn, while $B_{p,n}$ represents the downwash velocity at P due to a unit intensity doublet in the wake strip n. For an M x N panel lifting surface, P takes M x N different values and the problem reduces to a set of simultaneous, linear algebraic equations

$$4\pi \{w\} = [c]\{K\}, \quad (4.6)$$

where

$$C_{P,mm} = \begin{cases} A_{P,mn} & , \; m \neq M \\ A_{P,mn} + B_{P,n} & , \; m = M \end{cases}$$

The flow tangency condition, as detailed later, requires the downwash velocity induced by the doublets to equal the downward velocity of the wing at every point. Consequently, for prescribed wing motion and geometry, eq. (4.6) may be solved for the doublet distribution, K.

The proper approach to the solution of eq. (4.6) is to determine not only the doublet distribution but the wake geometry as well since it is known a priori. This additional requirement can increase computational effort appreciably. However, for moderate to high aspect ratio fixed wings it has been found sufficiently accurate to specify the wake to be a planar vortex sheet rather than to calculate its actual shape. A similar approach is therefore chosen for the rotor wake. That is, in the interest of reducing computer time without compromising accuracy, the rotor wake will be prescribed rather than calculated. The difficulty, however, lies in choosing the proper wake shape for a given flight condition. The strip theory model is simple but not physically realistic since it ignores wake curvature. The classical wake model is an improvement, but it neglects tip vortex effects and the contraction of the wake of the wake beneath the rotor disc. Only Landgrebe's experimentally determined rotor wake model

includes all of these important effects. He models the wake as having a strong tip vortex and a weaker inboard vortex sheet and gives empirical equations for the radial and axial coordinates of both as functions of rotor geometry and operating conditions. The details of the equations were presented in Ref. 55. In this report these equations were used with some slight modifications. The first modification was to extend the outer vortex sheet boundary to the tip vortex, since there is likely a physical connection between the two. The second was to simulate the roll up of the the vortex sheet into a tip vortex by gradually combining the outer vortex sheet wake strips into a single strip with the combined strength of the composite strips. This process was done over an arbitrarily chosen one-sixth rotor revolution to insure that the tip vortex reached full strength before passing beneath the following blade. The portion of the wake which combined to form the tip vortex was determined by the spanwise location of the peak load on the rotor blade, and since the peak load is generally near the 85-90% radius position, all wake strips outboard of that location were blended into the tip vortex. Furthermore, the outermost segment of the strips in this region was assigned tip vortex coordinates, while all others were given vortex sheet coordinates. It was also assumed that the vortex sheet contracted radially at the same rate as the tip vortex.

The blade surface is divided into a number of small panels and the panel size is smaller in regions where K varies most rapidly, i.e., near the blade edges. The freestream velocity is assumed to be constant across a panel and equal to the velocity at the geometric centroid of the panel. This velocity varies with

span due to the nature of the rotor flow field. Extending from each trailing edge panel is a wake strip whose coordinates are determined by Landgrebe's equations (Fig. 6 shows the panel approximation of the rotor blade and the modified wake model).

Calculation of Influence Coefficients

Eq. (4.6) can be solved for K at a discrete number of points on the surface which, placed at the geometric centroid of each panel. The influence of a surface panel on a collocation point is given by eq. (4.5a), which is evaluated numerically using a two-dimensional Gaussian quadrature. The influence of a wake strip on a collocation point is given by eq. (4.5b) with the following modification: implicit in the use of (4.3) for enforcing the zero-pressure condition in the wake is the assumption that the local streamlines are in the direction of the positive X-axis. In a linearized sense this is true for fixed wings. However, for rotary wings the streamlines are directed roughly helical paths beneath the rotor disc. To reflect this difference eq. (4.3) is therefore modified to

$$K(S) = K(S_{te})\, e^{-i\nu(S-S_{te})}, \qquad (4.7)$$

where S is the distance measured along the centerline of any wake strip. Of course, eq. (4.5b) must be changed in accordance with eq.(4.7). The effect that a particular wake strip has on a collocation point is therefore computed by adding the effect that each panel in the strip has on that point using the modified form of eq.(4.5b). As with the surface panels, the integrations are carried out with a two-dimensional Gaussian quadrature.

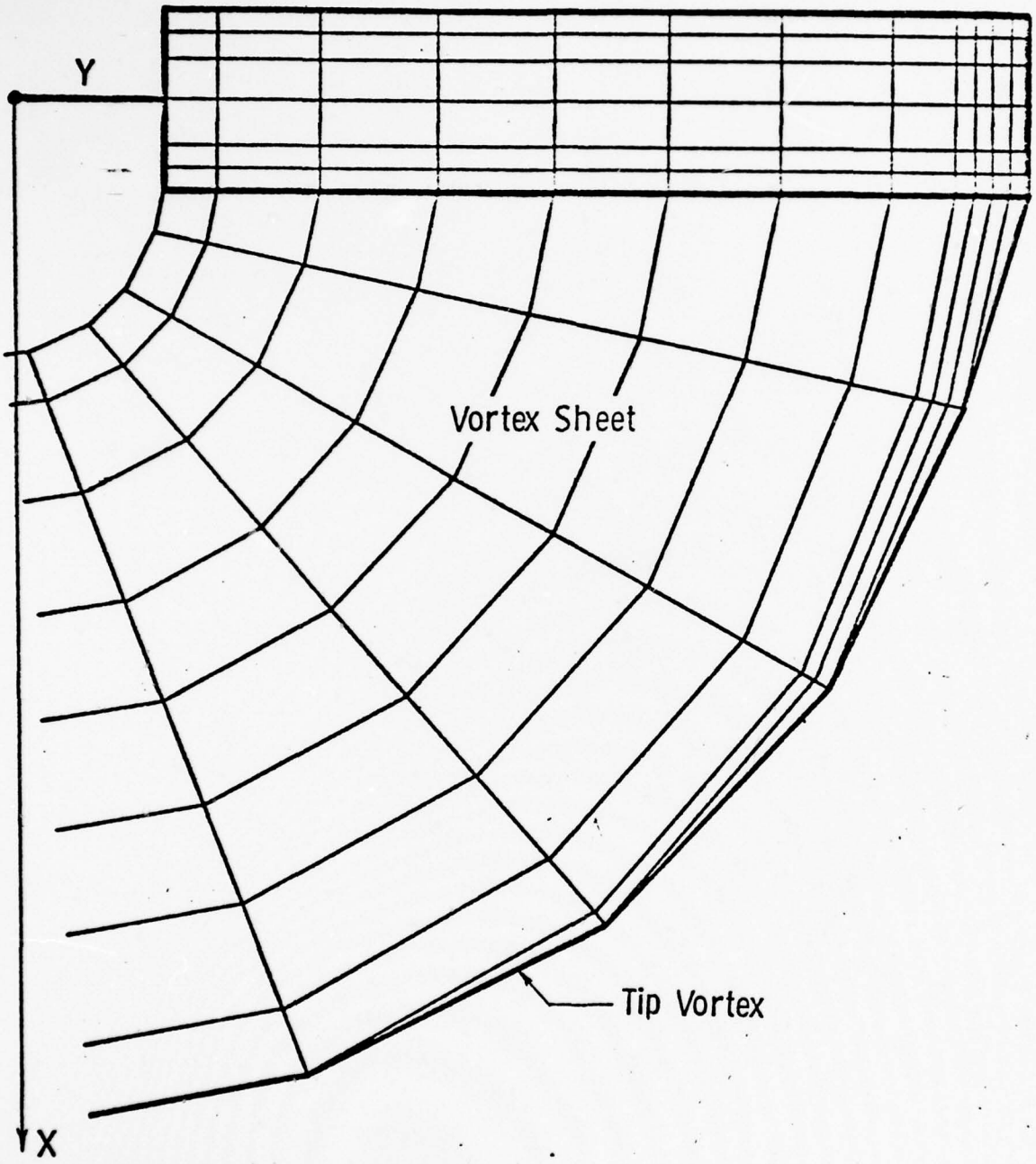

Figure 6. Rotor and Wake Model

Surface Boundary Condition

The vertical displacement of the blade is assumed to have a steady-state component due to coning and angle of attack, and an unsteady component due to flapping and twisting about this stady position, i.e.,

$$\zeta = \zeta_s + \zeta_b' e^{i\omega T} + \zeta_t' e^{i\omega T} \tag{4.8}$$

It can be seen from Fig. 7 that

$$\zeta_s = (e-y)\beta_c + x\alpha \tag{4.9a}$$

$$\zeta_b' = b(y)\, z_{tip} \tag{4.9b}$$

$$\zeta_t' = F(y)\, \alpha_{tip} \tag{4.9c}$$

The relations between the downwash velocity w_p and ζ, and w_p and the transformed downwash velocity W_p are, respectively,

$$w_p = \frac{\partial \zeta}{\partial t} + U \frac{\partial \zeta}{\partial x} \tag{4.10}$$

and

$$W_p = w_p \frac{e^{-i(\lambda x + \omega T)_p}}{U_t \beta_p} \tag{4.11}$$

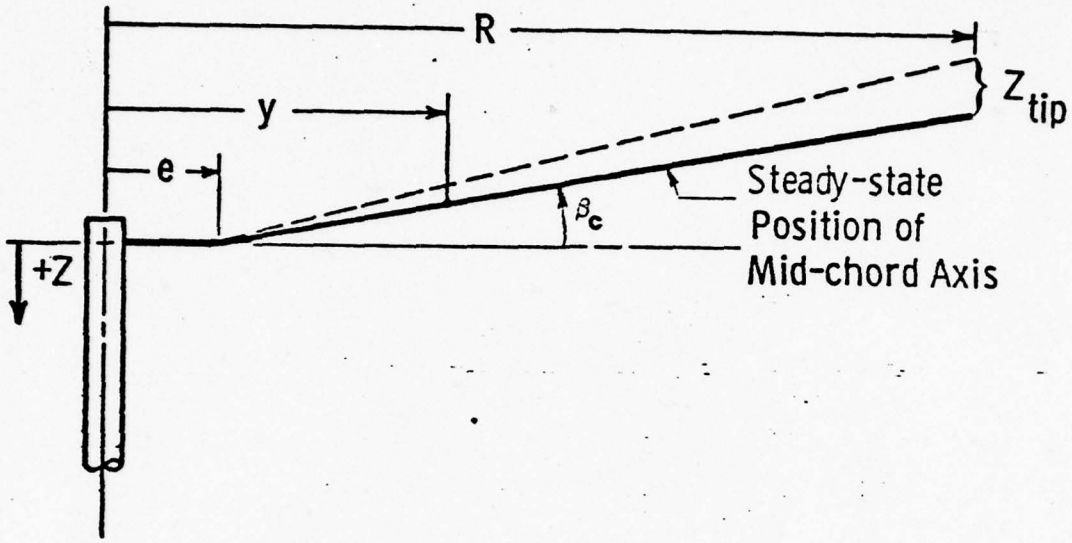

View from Trailing Edge

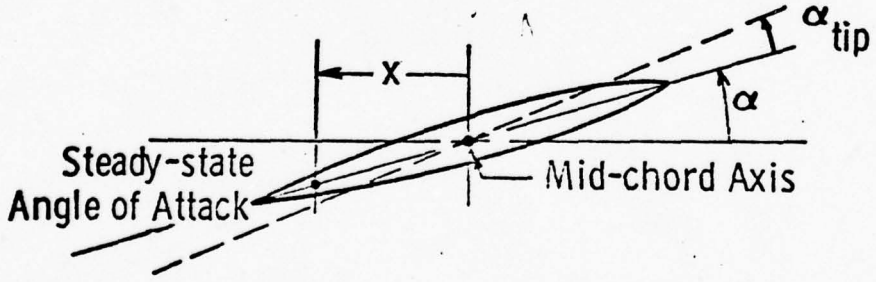

View from Blade Tip

Figure 7. Components of Rotor Blade Motion

Eqs.(4.8) through (4.11) are combined to give

$$W_p = W_{sp} + W_{zp} + W_{\alpha p} \quad , \tag{4.12}$$

where

$$W_{sp} = \frac{\dot{p}}{R\beta_p}\alpha_p \tag{4.12a}$$

$$W_{zp} = \frac{b(y)\, z_{tip}\, e^{-i\lambda_p x_p}}{R\beta_p}(i\epsilon) \tag{4.12b}$$

$$W_{\alpha p} = \frac{F(y)\,\alpha_{tip}\, e^{-i\lambda_p x_p}}{R\beta_p}\left(\alpha_p + i\epsilon\,\alpha_p\right). \tag{4.12c}$$

The solution for steady flow is obtained by setting $\lambda=0$ and $\lambda=0$ in eqs.(4.5a) and (4.5b) and using eqs. (4.6) and (4.12a). Similarly, the solutions for flapping and twisting are obtained by using eqs.(4.12a) and (4.12b), respectively in eq.(4.6).

Aerodynamic Loads

Eq.(4.2), the linearized expression for the lift in transformed coordinates, is modified to

$$\tilde{\ell}(X,Y,T) = \rho U U_t\left(i\omega K + \frac{\partial K}{\partial X}\right)e^{i(\lambda X+\omega T)} \tag{4.13}$$

By integrating eq.(4.13) along the chord, the local lift and moment per unit span may be expressed as

$$L' = \rho U^2 \ell\left(\frac{R}{y}\right)\left[\bar{K}_{te} - i\omega\int_{-1}^{1}\bar{K}\,dx\right]e^{i\omega T} \tag{4.14}$$

$$M'_{c/2} = -\rho U^2 \ell^2\left(\frac{R}{y}\right)\left[\bar{K}_{te} - \int_{-1}^{1}\bar{K}\,dx + i\omega\int_{-1}^{1}\bar{K}\,x\,dx\right]e^{i\omega T} \quad , \tag{4.15}$$

where $\bar{K} = Ke^{i\lambda x}$.

The unsteady lift and moment coefficients for flapping and twisting motions are expressed as

$$C_L = \frac{L'}{\rho U^2 \ell} = C_{Lz} z'_{tip} + C_{L\alpha} \alpha_{tip} \qquad (4.16)$$

$$C_{mc/2} = \frac{M'_{c/2}}{\rho U^2 \ell^2} = C_{Mz} z'_{tip} + C_{M\alpha} \alpha_{tip} , \qquad (4.17)$$

where $z'_{tip} = z'_{tip}/\ell$. It should be noted that C_{Lz}, $C_{L\alpha}$, C_{Mz}, and $C_{M\alpha}$ are complex quantities.

Solution Procedure

For a given rotor geometry and flight condition, blade element theory is used to calculate an initial guess to the rotor thrust coefficients, C_T. Based on this value of C_T and the initial conditions an initial wake shape is prescribed using the modified Landgrebe model. The resultant steady-state airloads are then calculated and an improved guess for C_T is made. If this second value differs appreciably from the first, a new wake geometry exists which is compatible with the steady-state load distribution, i.e., $\Delta C_T \to 0$. The unsteady aerodynamic derivatives are then calculated based on this converged geometry.

Results

Steady airloads and unsteady aerodynamic derivatives were calculated for an XH-51A helicopter rotor in hover. This rotor was chosen because experimental data[57] for the steady-state load distribution was available for comparison with theory.

The blade geometry and flight conditions were:

$$NB = 4, \quad R = 17.5', \quad c = 1.08', \quad y_{co} = 2.33',$$
$$\theta_1 = -5^\circ, \quad \theta_r = 10.61^\circ,$$
$$N_R = 355 \ (M_{tip} = 0.58).$$

In the unsteady case the blades were assumed to undergo rigid flapping and torsional motion such that

$$f(y) = \begin{cases} 0 & , y \leq e \\ \dfrac{(y-e)}{(R-e)} & , y > e \end{cases}$$

and

$$F(y) = 1.$$

Figs. 8 and 9 show the calculated lift and moment distributions for the XH-51A using the present theory with the classical and Landgrebe wake models. Both models overpredict the overall blade lift although Landgrebe's model predicts the loading trends more accurately, specifically the load spike near the tip due to the tip vortex. The mean value for C_T for the classical model was 0.00577 and that for the Landgrebe model was 0.00584, while the experimental value was roughly 0.005 - - a difference of 15 to 17% between theory and experiment. This difference may be due to the approximate nature of the present method, i.e., discretizing the linear spanwise velocity field into constant velocity segments. No comparison was made between the theoretical and experimental moment distributions since the measured data were referenced to an unspecified axis. It might be expected,

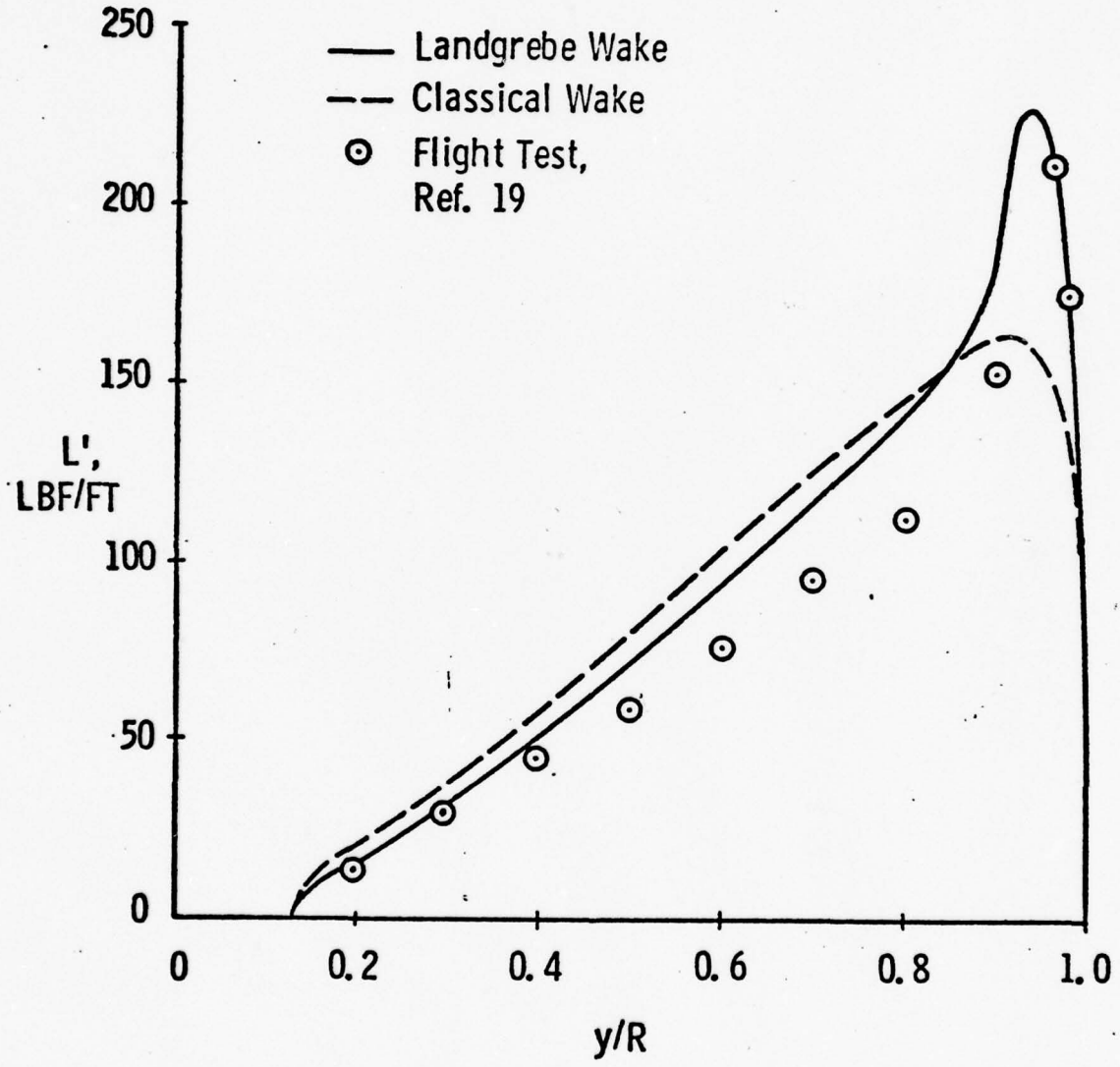

Figure 8. Lift per Unit Span, XH-51A Helicopter Rotor

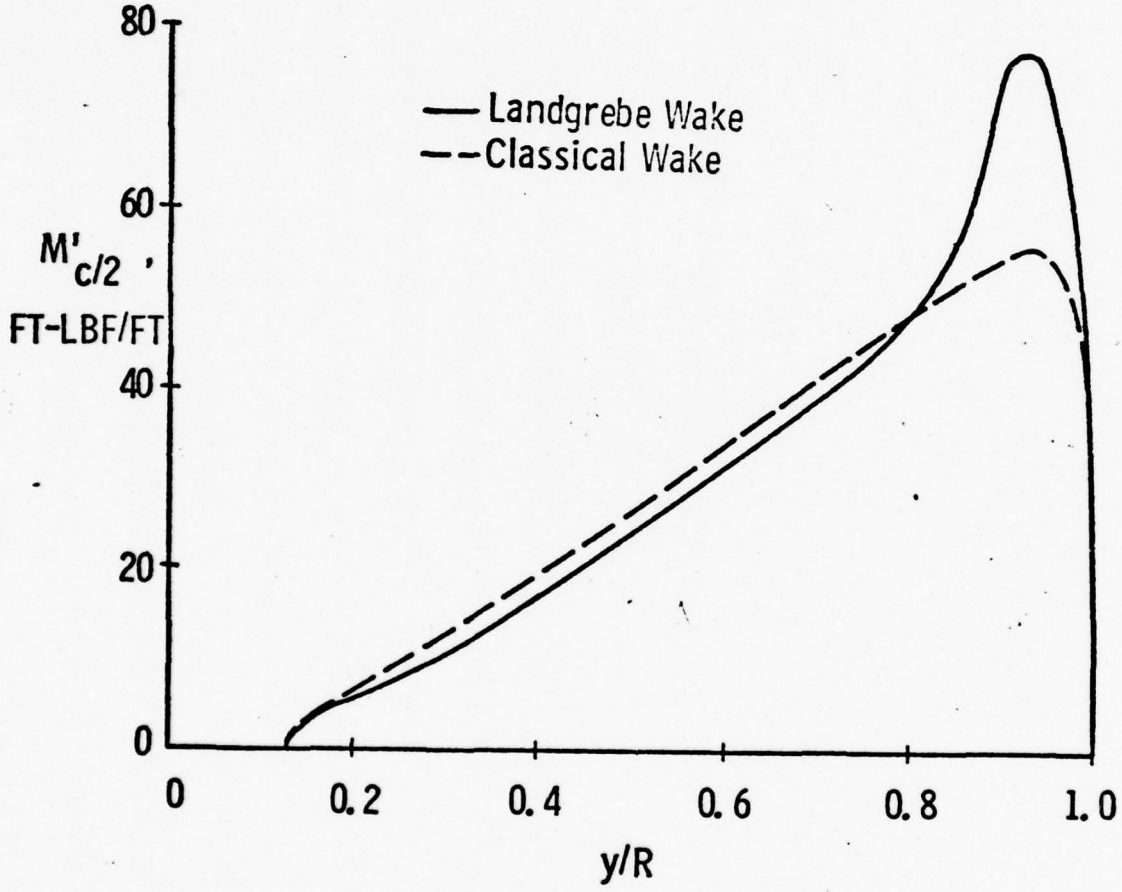

Figure 9. Moment per Unit Span, XH-51A Helicopter Rotor

however, that Landgrebe's model would give better results in the tip region than would be the classical model. The number of wake revolutions used in this study was varied from one to four with no appreciable change in the overall thrust or character of the loading curves, but with a drastic increase in computational time. The displyed results are therefore those obtained using a single wake revolution. For lightly loaded rotors (where the rotor wake is closer to the blade) it may be necessary to include more wake revolutions to get accurate results. The calculation of the steady state loads using either wake model required approximately 36 seconds of CPU time in G-Level FORTRAN on Amdahl 470V/6 computer.

Based on the steady-state results only the Landgrebe model was used for three frequency ratios shown in Figs.10 through 17. Evident in each of these figures is the strong tip vortex influence on the loading over the outer 20% of the blade. In the present study no attempt is made to explain the variation of these quantities as a function of frequency ratio or its significance in flutter analysis. However, based on the reasonable correlation between steady-state theoretical and experimental loading using the Landgrebe model, it is hoped that the computed unsteady aerodynamic derivatives will also be reasonably accurate. In the future these results will be compared with those of strip theory and classical wake model representations and applied to investigate their effect on aeroelastic stability boundaries as was done in Ref. 58. The calculation of the steady-state airloads and wake geometry and the resulting unsteady aerodynamic derivatives required approximately 2.8 minutes of CPU time in G-Level FORTRAN

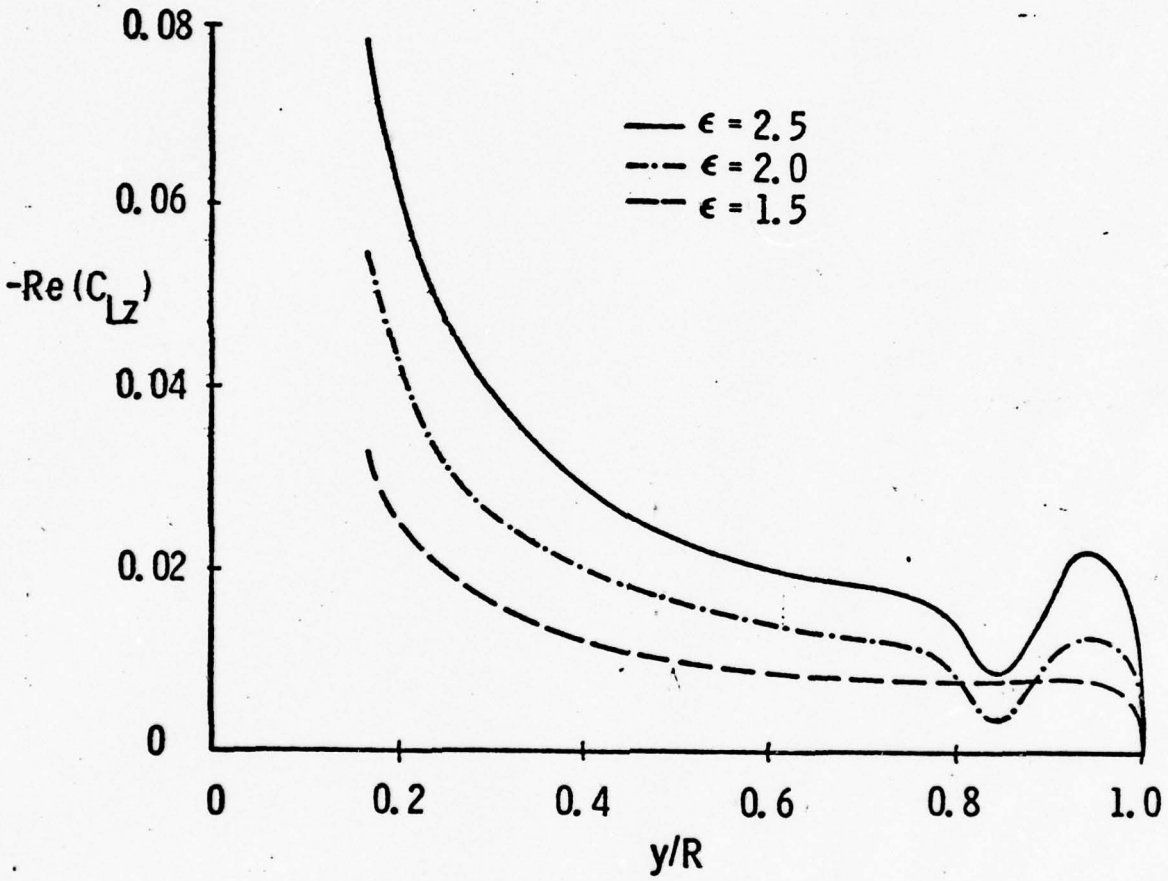

Figure 10. Real Part of Lift Due to Flapping

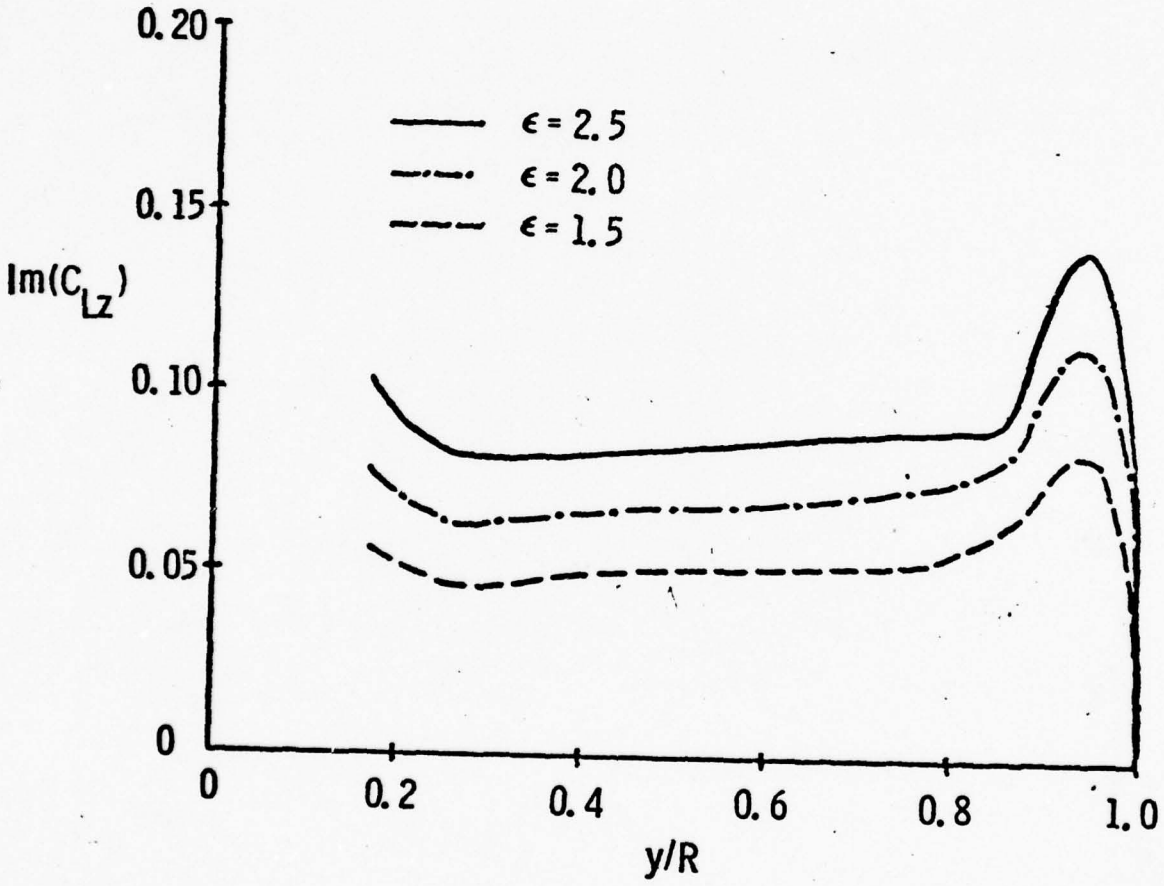

Figure 11. Imaginary Part of Lift Due to Flapping

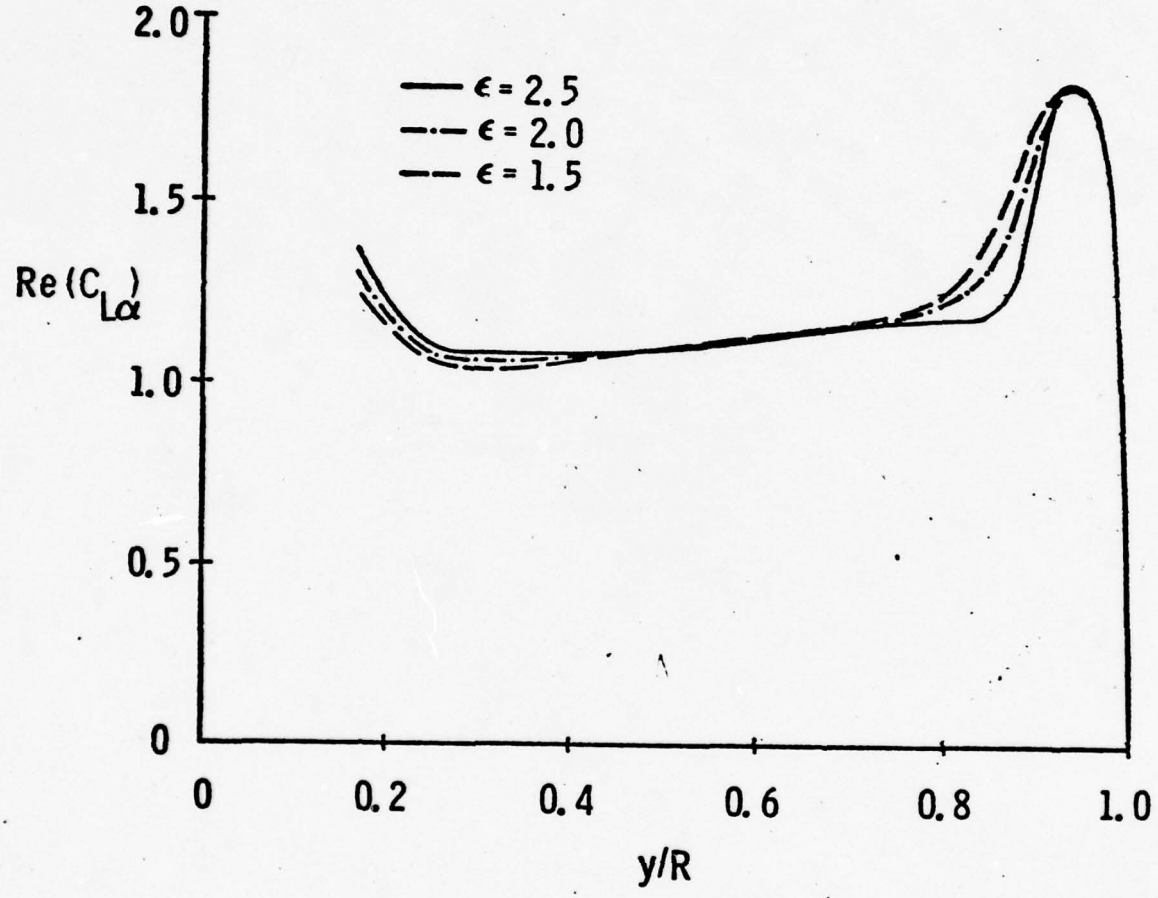

Figure 12. Real Part of Lift Due to Torsion

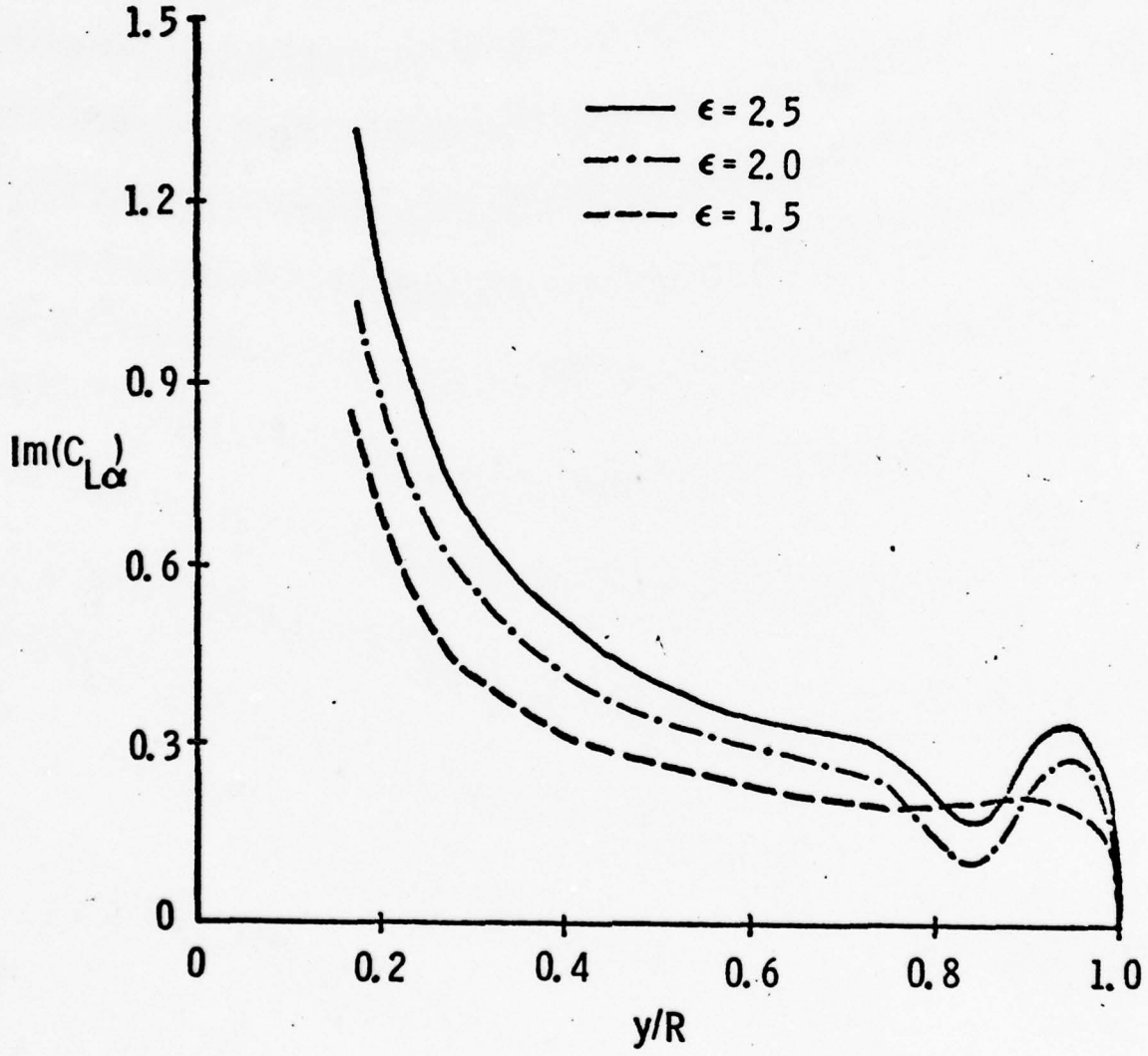

Figure 13. Imaginary Part of Lift Due to Torsion

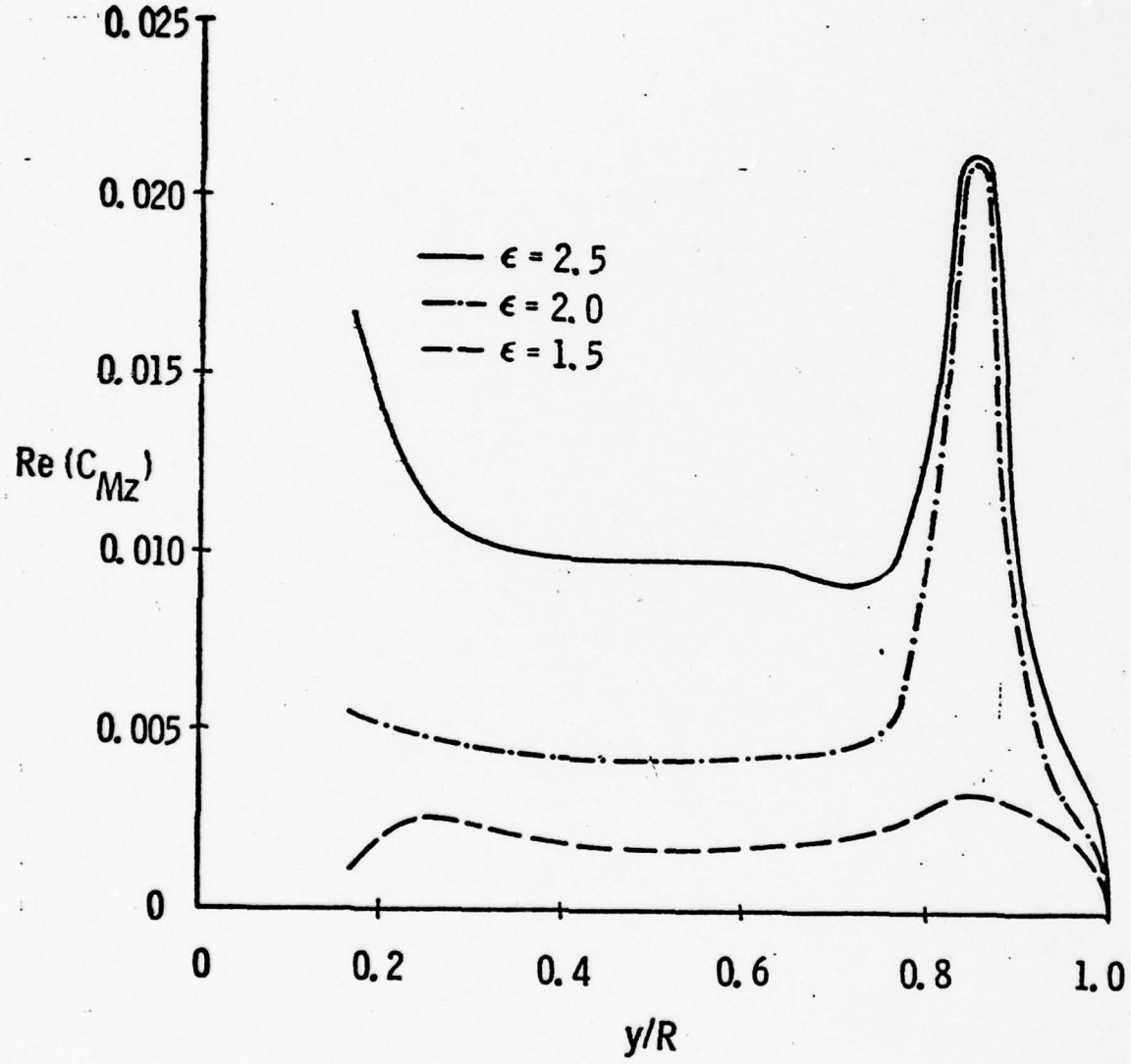

Figure 14. Real Part of Moment Due to Flapping

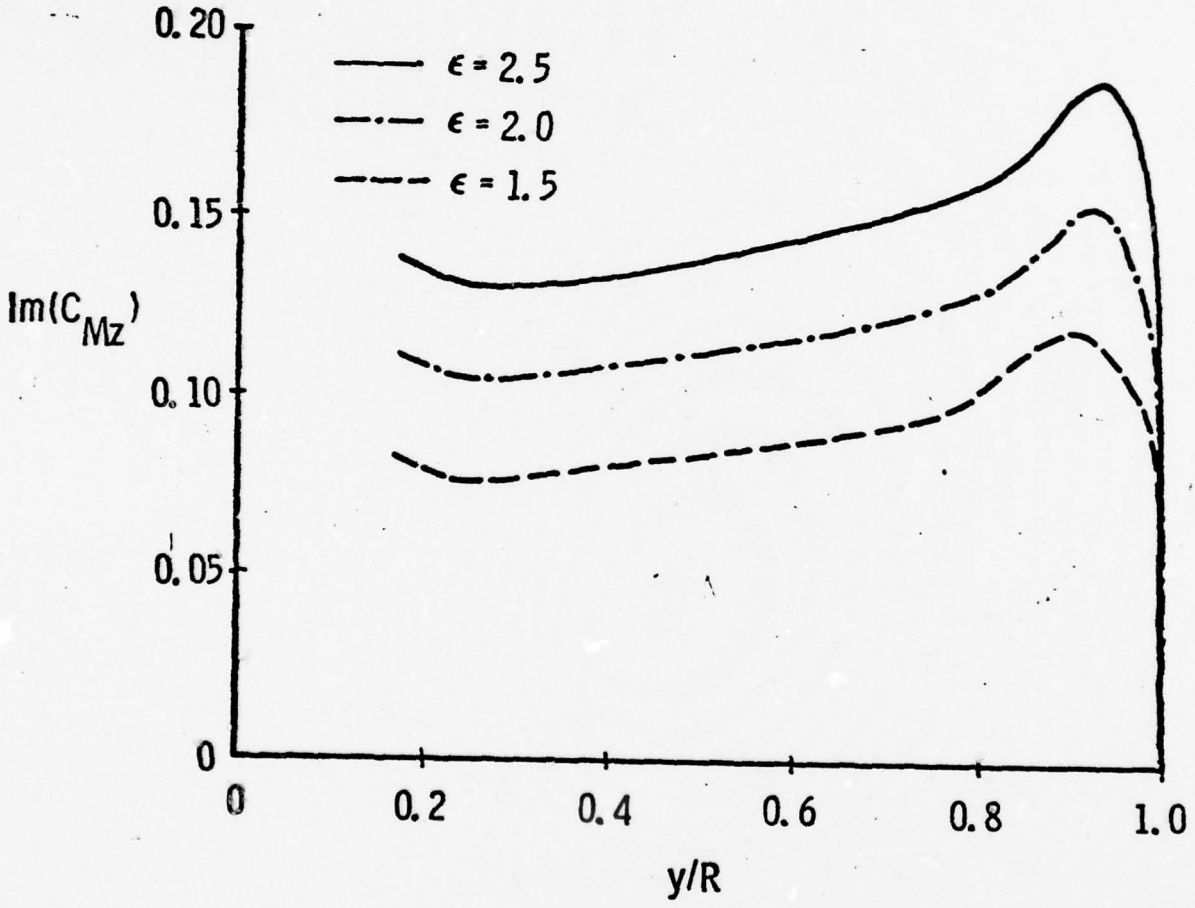

Figure 15. Imaginary Part of Moment Due to Flapping

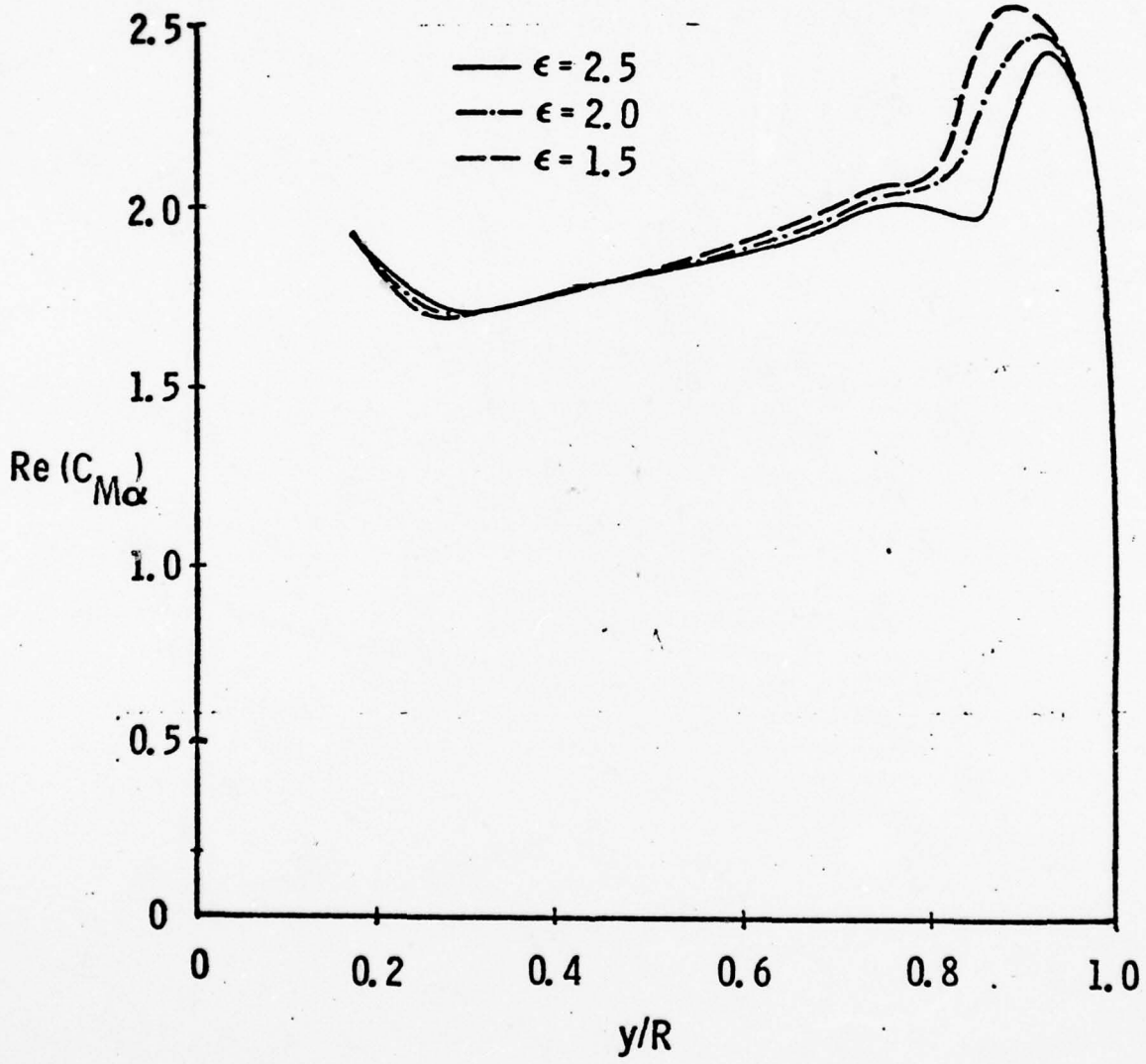

Figure 16. Real Part of Moment Due to Torsion

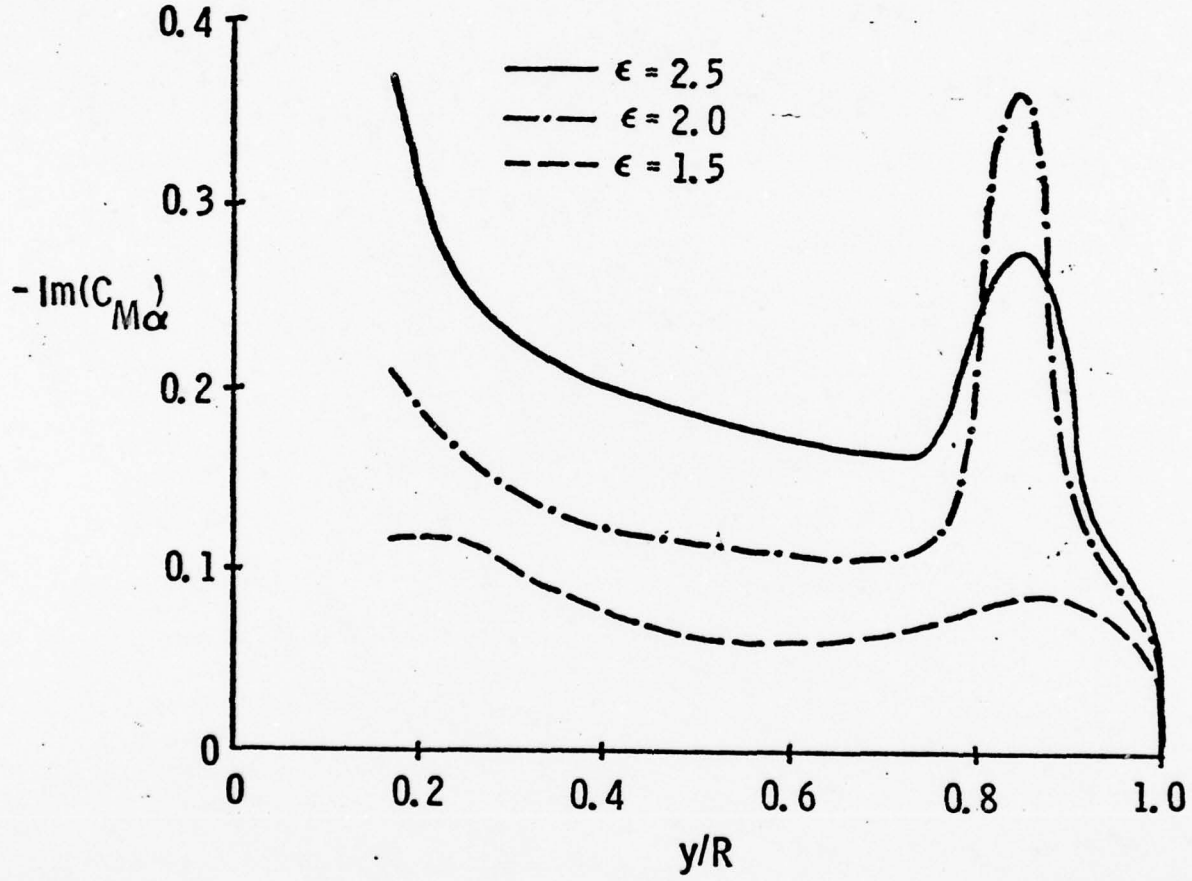

Figure 17. Imaginary Part of Moment Due to Torsion

on an Amdahl 470V/6 computer.

Conclusions

A velocity potential lifting surface method has been used in conjunction with a realistic rotor wake model to compute the steady airloads and unsteady aerodynamic derivatives for an arbitrary hovering rotor in compressible subsonic flow. The theoretical results compare well with experimental data for four-bladed rotors, suggesting that unsteady loads calculated with the same wake geometry may also be reasonably accurate. With the proper choice of flappinf and torsional modes, the present method could be used to generate aerodynamic derivatives for use in flutter analysis. In fact the next section deals with this topic.

iii) Aeroelastic Analysis of a Single-Bladed Rotor

The unsteady aerodynamic analysis and the computer program described in the previous section is applied to predict the flutter speed of a single-blades rotor in Ref. 59. The results and the discussion of this analysis is presented in this section.

A single-bladed rotor with the following geometric and structural properties was considered:

Radius	-	25.0'	
Chord	-	2.0'	
Y_{co}	-	2.5'	
r_α^2	-	0.25	(radius of gyration^2)
ω_b/ω_α	-	0.50	(bending/torsion freq. ratio)
μ	-	80.0	(density ratio)
c.g. loc.	-	0.1	(aft of elastic axis)

$0.0 \leq \omega \leq 0.5$

To assure compatibility between the two and three-dimensional aerodynamic derivatives, a classical wake was prescribed in the three dimensional analysis. The use of classical wake resulted in no loss in generality of the three-dimensional theory since it has been shown that there is little difference between the results obtained from using either Landgrebe's wake model or a classical wake (Ref. 59).

The principal flutter parameters in this analysis were the location of the elastic axis (a) and the bending/torsion frequency ratio (ζ). The varation of flutter speed is shown in Fig. 18 for the assumed blade section at 0.75 R, using both two- and three-dimensional aerodynamics. Using two-dimensional aerodynamics for locations of the elastic axis ahead of the quater chord, an analyst could mistakenly conclude that there is no chance for flutter to occur; for this case the three-dimensional aerodynamics indicates a lower flutter speed. However, when the elastic axis is moved aft of a = 0.3, three-dimensional aerodynamics is less conservative than two-dimensional aerodynamics. Consequently, two-dimensional theory should be used.

For the rest of this study, the elastic axis was located at a = 0.2. Fig. 19 shows the variation of the flutter speed with the ratio of the bending/torsion frequencies. It is seen that two-dimensional theory predicts a lower flutter speed than does the three-dimensional theory for all values of ζ. Also, for values of ζ near 1.0 and greater, both aerodynamic theories predict no flutter for values of reduced frequecy less than 0.5 These same trends are also seen when the flutter frequency is

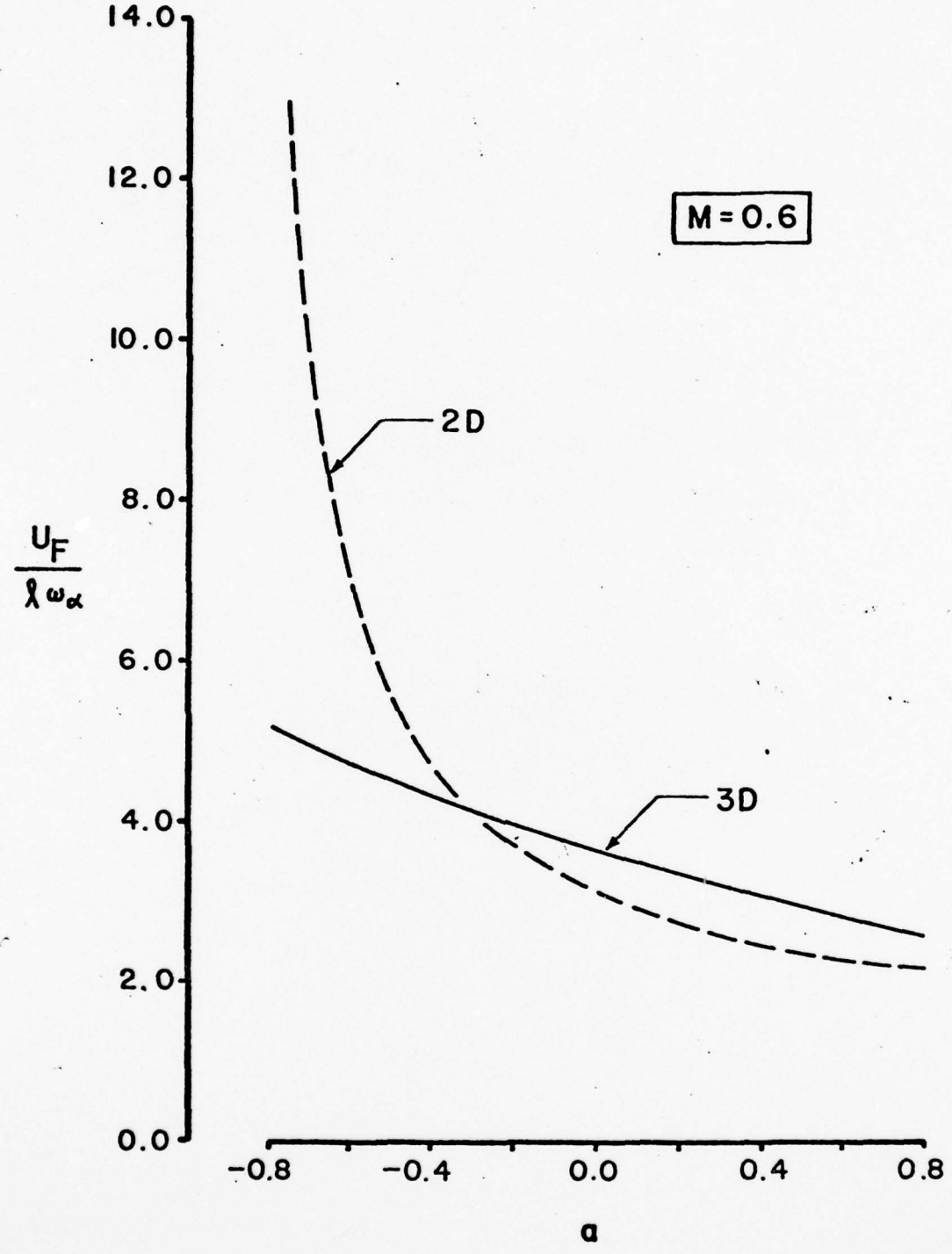

Figure 18. Effect of the Elastic Axis Location on the Flutter Speed

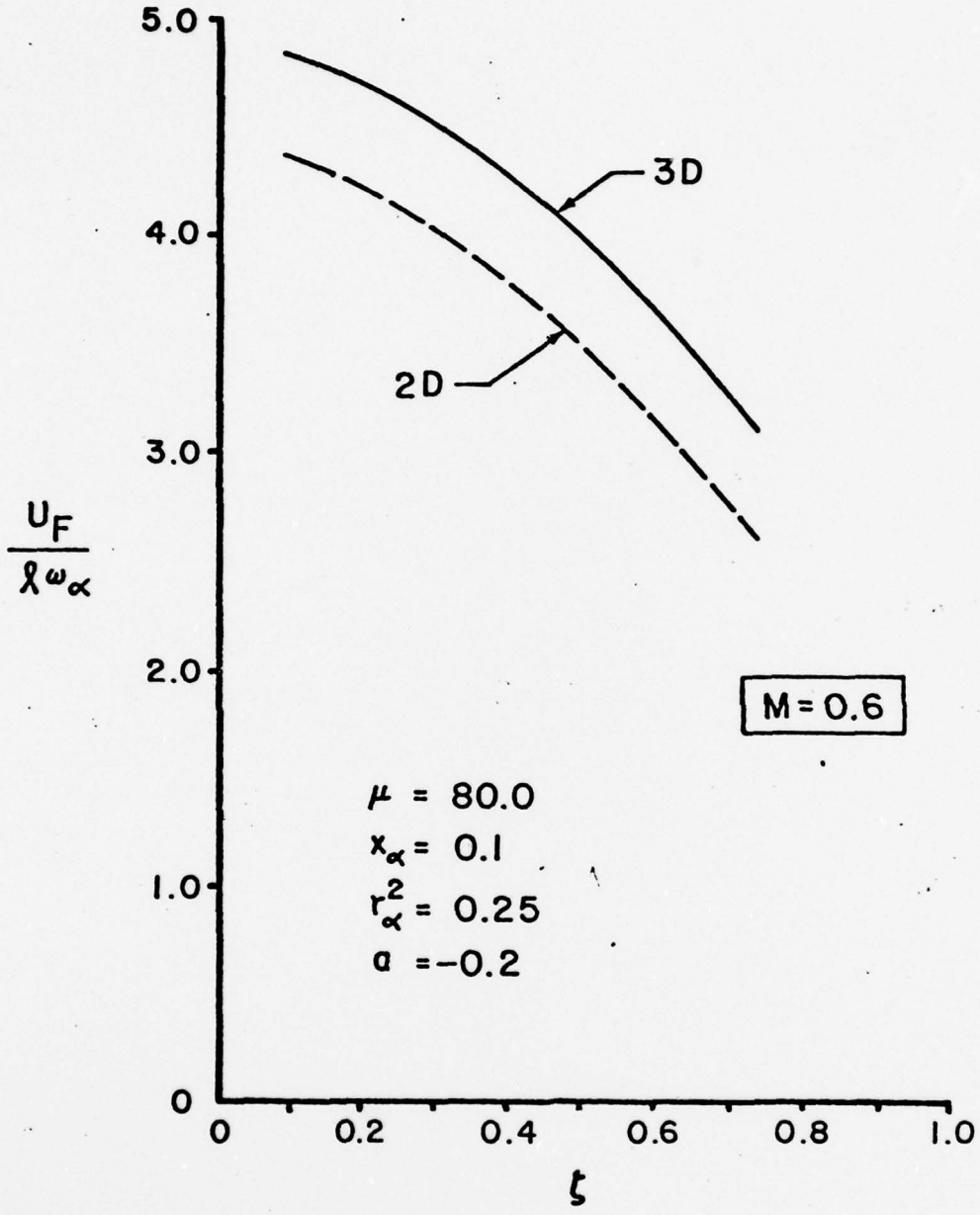

Figure 19. Variation of Flutter Speed with the Bending/Torsion Frequency Ratio

plotted against the bending/torsion frequency ratio (Fig. 20). In terms of a rotor system, these results indicate that no flutter condition will be encountered for the bending stiffness greater than the torsional rigidity. Further from these two figures, one can conclude that the finite aspect ratio effects are such that they reduce the flutter speeds.

Fig. 21 shows the variation of the flutter speed with the density ratio. For both cases, the flutter speed increases with an increase in the density ratio, and the gradient for the two-dimensional curve is seen to be decreasing faster than that of the three-dimensional curve. The trend indicates that the increase in density ratio has a slightly less stabilizing effect on the airfoil motion when using two-dimensional airfoil theory. Thus, for high values of density ratio, a very conservative flutter speed may be predicted using strip theory.

The varaition of the flutter speed with the square of the non-dimensional radius of gyration is shown in Fig. 22. Once again, the flutter speed obtained using strip theory is the conservative result. The flutter speed increses as the radius of gyration increases.

The varaition of c.g. location on the flutter speed is shown in Fig. 23. Here, using three-dimensional aerodynamic derivatives, there is insignificant variation in the flutter speed. However, for strip theory, the effect of c.g. location variation has a much more pronounced effect on the flutter speed.

The results presented in this section are very preliminary

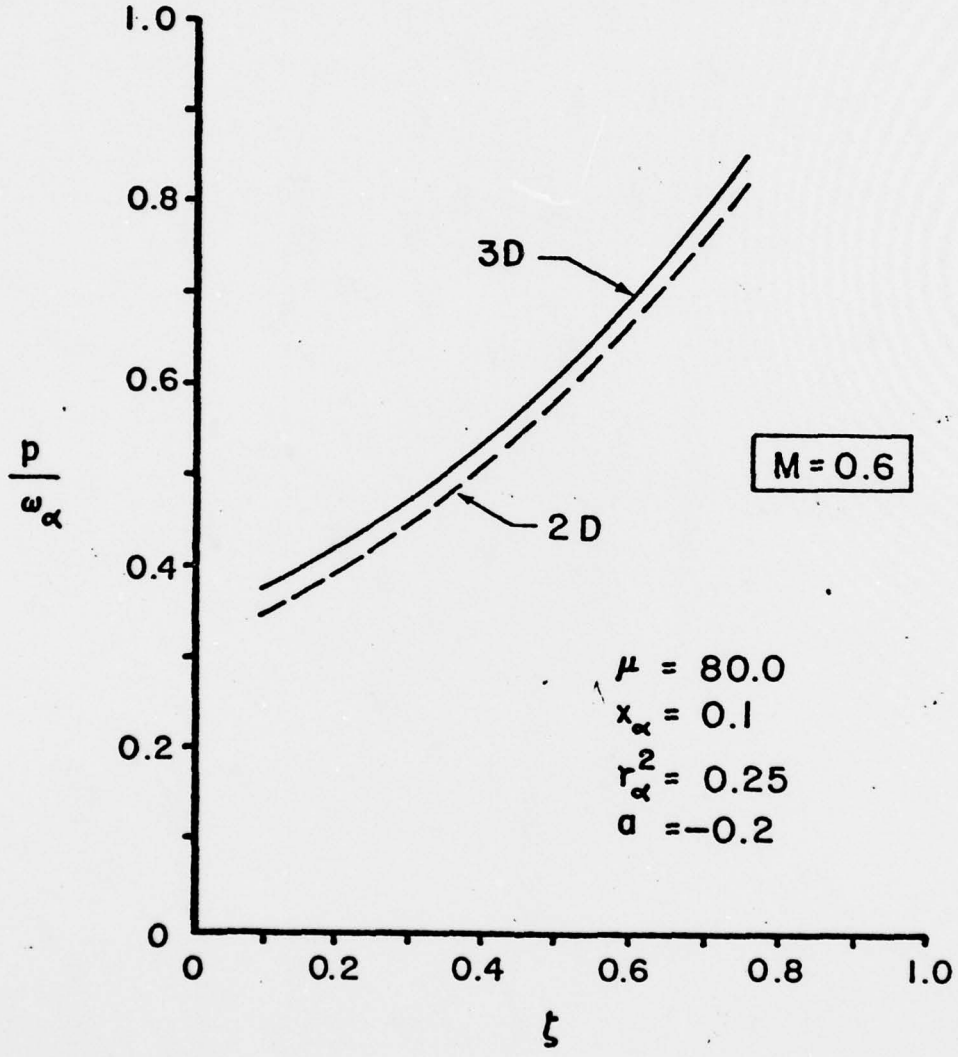

Figure 20. Variation of Flutter Frequency with the Bending/Torsion Frequency Ratio

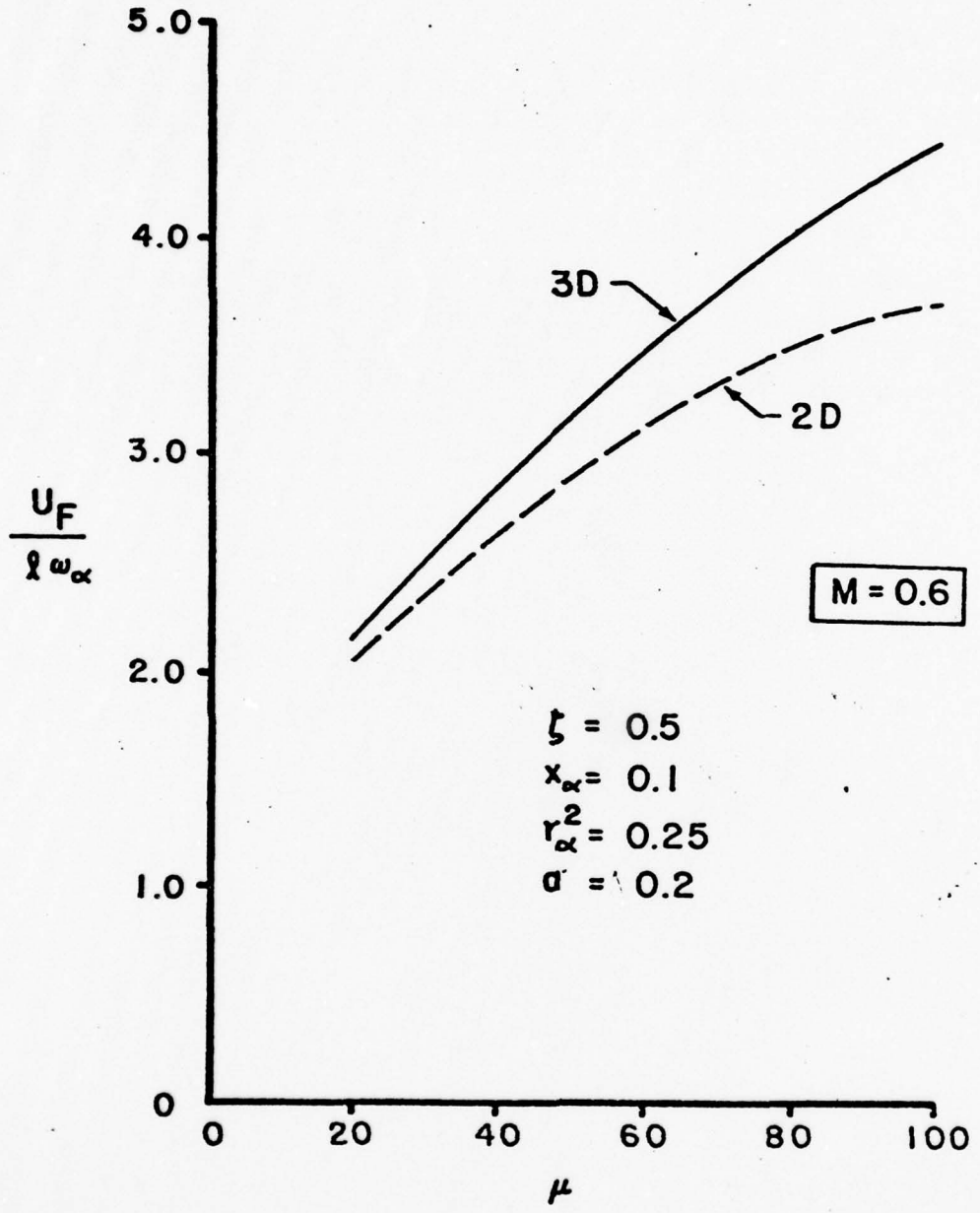

Figure 21. Effect of the Density Ratio on the Flutter Speed

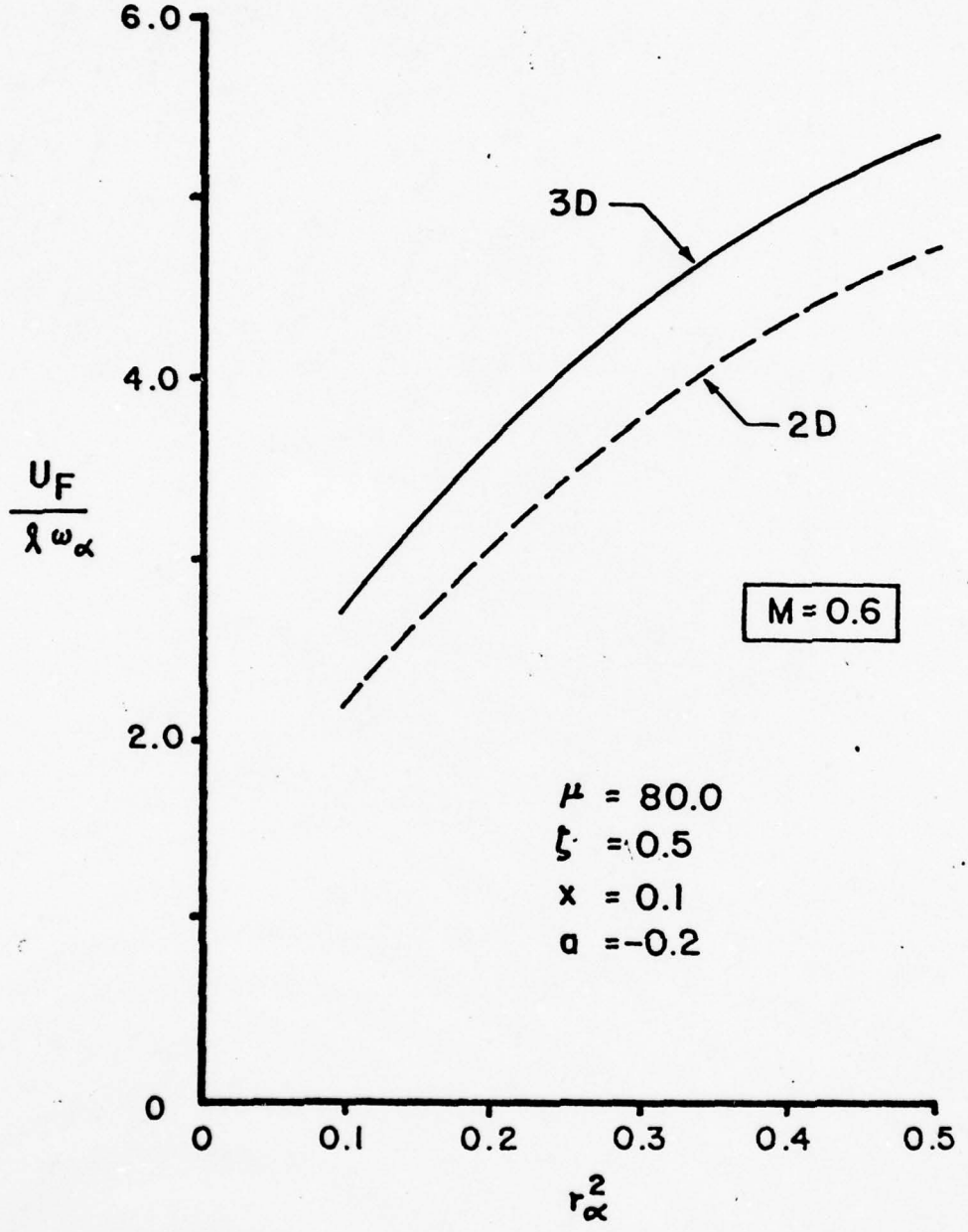

Figure 22. Variation of the Flutter Speed with the Square of the Radius of Gyration

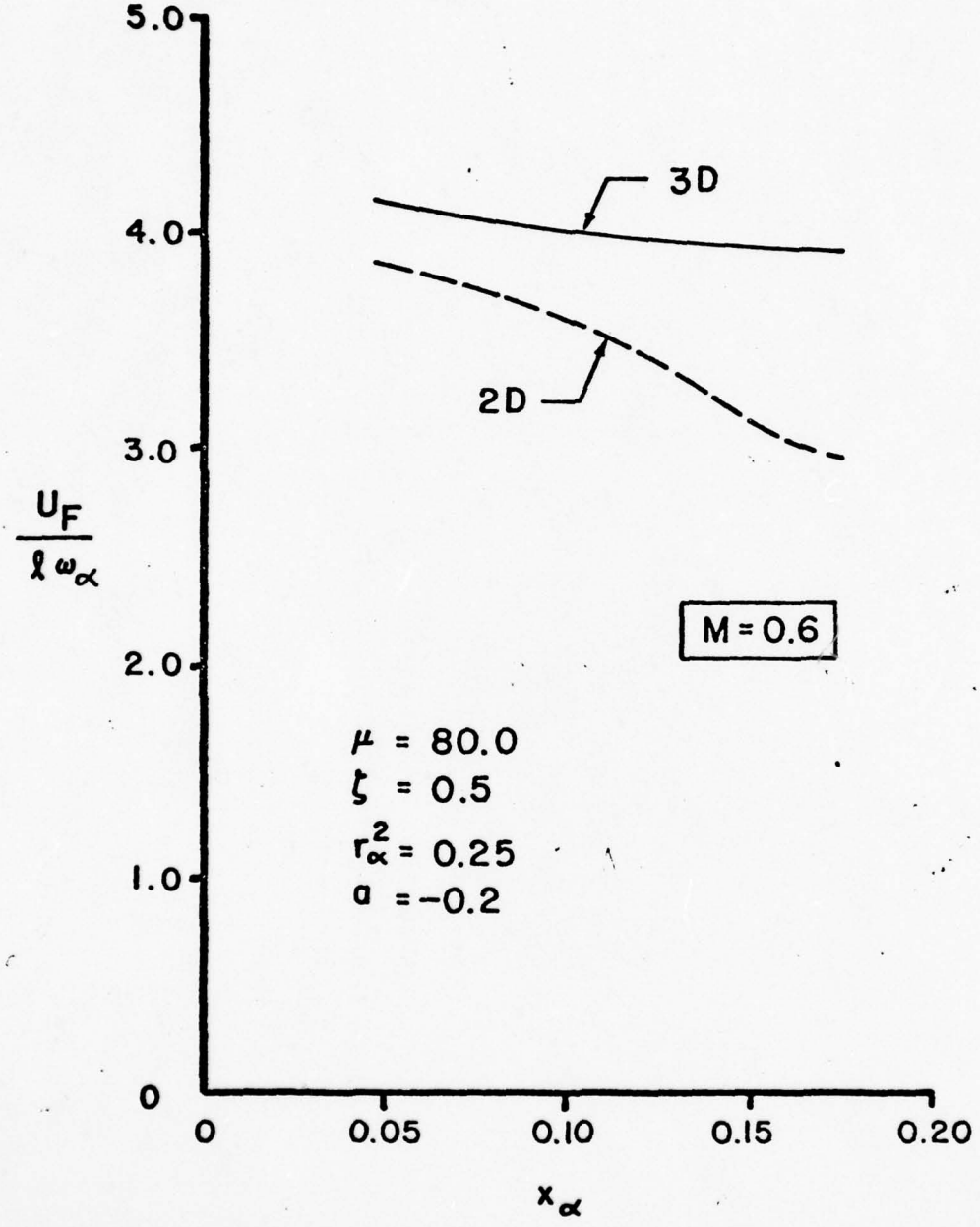

Figure 23. Variation of the Flutter Speed with Movement of the Center of Gravity

and one has to be very careful before making any general or conclusive statements. An extensive parametric study is needed.

REFERENCES

1. Hazen, D. C., "The Rebirth of Subsonic Aerodynamics," Astronautics and Aeronautics, Nov. 1967

2. Kocurek, J. D., "A New Finite Element Lifting Surface Technique," M.S. Thesis, Texas A&M University, May 1973.

3. Bisplinghoff, R. L., Ashley, H., and Halfman, R. L., Aeroelasticity, Addison-Wesley, Reading, Mass., 1955, pp. 229-243.

4. Campbell, G. S., "A Finite-Step Method for the Calculation of Span Loadings of Unusual Plan Forms," RM L50L13, July 1951, NACA.

5. Blackwell, J. A., Jr., "A Finite-Step Method for Calculation of Theoretical Load Distributions for Arbitrary Lifting-Surface Arrangements at Subsonic Speeds," TN D-5335, July 1969, NASA.

6. Ashley, H., Widnall, S., and Landahl, M. T., "New Directions in Lifting-Surface Theory," AIAA Journal, Vol. 3, No. 1, Jan. 1965, pp. 3-16.

7. Landahl, M. T., and Stark, V. J. E., "Numerical Lifting-Surface Theory Problems and Progress," AIAA Journal, Vol. 6., No. 11, Nov. 1968, pp. 2049-2060.

8. Jones, W.P., and Rao, B. M., "Airloads and Moments on an Aircraft Flying over a Pair of Inclined Trailing Vortices," Aircraft Wake Turbulence, Plenum Publishing Corporation, New York, 1971, pp. 523-545.

9. Falkner, V. M., "The Calculation of Aerodynamic Loading on Surfaces of Any Shape," R&M 1910, 1943, British Aeronautical Research Council

10. Woodward, F. A., "Analysis and Design of Wing-Body Combinations at Subsonic and Supersonic Speeds," Journal of Aircraft, Vol. 5, No. 6, Nov-Dec. 1968, pp. 528-534.

11. Soncrant, C. U., "Application of the Vortex-Box Method to the Unsteady Incompressible Flow over Finite Wings," M. S. Thesis, Texas A&M University, May 1973.

12. Albano, E., and Rodden, W. P., "A Doublet-Lattice Method for Calculating Lift Distirbutions on Oscillating Surfaces in Subsonic Flows," AIAA Journal, Vol. 7, No. 2, Feb. 1969, pp. 279-285.

13. Kalman, T. P., Rodden, W. P., and Giesing, J. P., "Application of the Doublet-Lattice Method to Nonplanar Configurations in Subsonic Flow," AIAA Paper No.70-539, 1970.

14. Chang. C. C., and Chu, W. H., "Aerodynamic Interference of Cascade Blades in Synchronized Oscillation," Journal of Applied Mechanics, Dec. 1955, pp. 503-508.

AD-A052 417 TEXAS A AND M UNIV COLLEGE STATION F/G 20/4
THE DEVELOPMENT AND APPLICATION OF A SIMPLE METHOD FOR DETERMIN--ETC(U)
FEB 78 B M RAO, V ELCHURI, P R SCHATZLE DAHC04-74-G-0184
UNCLASSIFIED ARO-11695.2-E NL

2 OF 2
AD
A052417

END
DATE
FILMED
6-78
DDC

15. Schorr, B., and Reddy, K. C., "Inviscid Flow Through Cascades in Oscillatory and Distorted Flow," AIAA Journal, Vol. 9, No. 10, Oct. 1971, pp. 2043-2050.

16. Jones, W. P., and Moore, J. A., "Flow in the Wake of a Cascade of Oscillating Airfoils, AIAA Journal, Vol. 10, No. 12, Dec. 1972, pp. 1600-1605.

17. Rao, B. M., and Jones, W. P., "Unsteady Airloads on a Cascade of Staggered Blades in Incompressible Flow," Proceedings of the Workshop on Unsteady Flows in Jet Engines, UARL, July 1974.

18. Runyan, H. L., and Watkins, C. E., "Considerations on the Effect of Wind-Tunnel Walls on Oscillating Air Forces for Two-Dimensional Subsonic Compressible Flow", NACA TN2552, Sep. 1951.

19. Jones, W. P., "Wind-Tunnel Wall Interference Effects on Oscillating Airfoils in Subsonic Flow," R&M 2943, British Aeronautical Research Council, Dec. 1953.

20. Lan, F., and Fiedman, M., "Theoretical Investigation of Subsonic Oscillatory Blade-Row Aerodynamics," NACA TN U136, Feb. 1958.

21. Fleeter, S., "Fluctuating Lift and Moment Coefficients for Cascaded Airfoils in a Nonuniform Compressible Flow," Journal of Aircraft, Vol. 10, No. 2, Feb. 1973, pp. 93-98.

22. Kaji, S., and Okazaki, T., "Propagation of Sound Waves Through a Blade Row; II. Analysis Based on the Acceleration Potential Method," Journal of Sound and Vibration, Vol. 11, No. 3, 1970, pp. 355-375.

23. Rao, B. M., and Jones, W. P., "Unsteady Airloads on a Cascade of Staggered Blades in Subsonic Flow," Presented at the 46th PEP Meeting on Unsteady Phenomena in Turbomachinery, AGARDOGRAPH 177, Sep. 1975.

24. Runyan, H. L., and Woolston, D. S., "Method for Calculating the Aerodynamic Loading on an Oscillating Finite Wing in Subsonic and Sonic Flow," NACA TR 1322, 1957.

25. Lawrence, H. R., and Gerber, E. H., "The Aerodynamic Forces on Low Aspect Ratio Wings Oscillating in an Incompressible Flow," Journal of theAeronautical Sciences, Vol. 19, No. 11, Nov. 1952, pp. 769-781.

26. Lawrence. H. R., "The Lift Distribution of Low-Aspect-Ratio Wings at Subsonic Speeds," Journal of the Aeronautical Sciences, Vol. 18, No. 10, Oct. 1957, pp. 683-695.

27. Garrick, I. E., "Some Research on High Speed Flutter," Proceedings of the Third Anglo-American Aeronautical Conference, Appendix B, 1951

28. Dengler, M. A., Goland, M., "The Subsonic Calculation of Circulatory Spanwise Loadings for Oscillating Airfoils by Lifting-Line Techniques," Journal of the Aeronautical Sciences, Vol. 19, No. 11, Nov. 1952, pp. 751-759.

29. Laidlaw, W. R., and Halfman, R. L., "Experimental Pressure Distributions on Oscillating Low Aspect Ratio Wings," Journal of the Aeronautical Sciences, Vol. 23, No. 2, Feb. 1956, pp. 117-124, p. 176.

30. Jones, W. P., McCrosky, W. J., and Costes, J. J., "Unsteady Aerodynamics of Helicopter Rotor Blades, NATO AGARD Report No. 595, April 1972.

31. Loewy, R. G., "A Two-Dimensional Approximation to the Unsteady Aerodynamics of Rotary Wings," Journal of the Aeronautical Sciences, Vol. 24, No. 9, February 1957, pp. 81-92.

32. Jones, J. P., "The Invluence of the Wake on the FLutter and Vibration of Rotor Blades," Aeronautical Quarterly, Vol. IX, August 1958.

33. Jones, W. P., "Aerodynamic Forces on Wings in Non-Uniform Motion," R&M No. 2117, 1945, British Aeronautical Research Council.

34. Daughaday, H. and Kline, J., "An Investigation of the Effect of Virtual Delta-Three Angle and Blade Flexibility on Rotor Blade Flutter," Cornell Aeronautical Laboratory Report, SB-86-2-5-2, August 1954.

35. Timman, R. and Van de Vooren, A. I., "Flutter of a Helicopter Rotor Rotating in its own Wake," Journal of the Aeronautical Sciences, Vol. 24, No. 9, September 1957, pp. 694-702.

36. Jones, W. P. and Rao, B. M., "Compressibility Effects on Oscillating Rotor Blades in Hovering Flight," AIAA Journal, Vol. 8, No. 2, February 1970, pp. 321-329.

37. Jones, W. P., "The Oscillating Airfoil in Subsonic Flow," R&M No. 2921, 1956, British Aeronautical Research Council.

38. Hammond, C. E., "Compressibility Effects in Helicopter Rotor Blade Flutter," GITAER Report 69-4, December 1969, Georgia Institute of Technology, School of Aerospace Engineering.

39. Ashley, H., Moser, HH., and Dugundji, J., "Investigation of Rotor Response to Vibratory Aerodynamic Inputs, Part III, Three-Dimensional Effects on Unsteady Flow through a Helicopter Rotor," WADC TR 58-87, October 1958, AD203392, U.S. Air Force Air Research and Development.

40. Reissner, E., "Effects of Finite Span on the Airload Distributions for Oscillating Wings, Part I - Aerodynamic Theory of Oscillating Wings of Finite Span," NACA Technical Note No. 1194, 1947.

41. Jones, W. P., and Rao, B. M., "Tip Vortex Effects on Oscillating Rotor Blades in Hovering Flight," AIAA Journal, Vol. 9, No. 1, January 1971, pp. 106-113.

42. Miller, R. H., "Unsteady Airloads on Helicopter Rotor Blades," Journal of the Royal Aeronautical Society, Vol. 86, No. 640, April 1964, pp. 217-229.

43. Miller, R. H., "On the Computation of Airloads Acting on Rotor Blades in Forward Flight," Journal of the American Helicopter Society, Vol. 7, No. 2, April 1962, pp. 55-66.

44. Miller, R. H., "Rotor Blade Harmonic Air Loading," AIAA Journal, Vol. 2, No. 7, July 1964, pp. 1254-1269.

45. Jenney, D. S., Olson, J. R., and Landgrebe, A. J., "A Reassessment of Rotor Hovering Performance Prediction Methods," Journal of the American Helicopter Society, Vol. 13, No. 2, April 1968, pp. 1254-1269.

46. Landgrebe, A. J., "An Analytical Method for Predicting Rotor Wake Geometry," Journal of the American Helicopter Society, Vol. 14, No. 4, October 1969, pp. 20-32.

47. Landgrebe, A. J., "An Analytical and Experimental Investigation of Helicopter Rotor Hover Performance and Wake Geometry Characteristics," USAAMRDL Technical Report 71-24, June 1971.

48. Piziali, R. A., "A Method for Predicting the Aerodynamic Loads and Dynamic Response of Rotor Blades," USAAV-LABS Technical Report 65-74, January 1966, AD 628583.

49. Sadler, S. G., "A Method for Predicting Helicopter Wake Geometry, Wake Induced Flow and Wake Effects on Blade Loads," presented at the 27th Annual National Forum of the American Helicopter Society, Washington, D.C., May 1972.

50. Ward, J. F. and Snyder, W. J., "The Dynamic Response of a Flexible Rotor Blade to a Concentrated Force Moving from Tip to Root," NASA TN D 5410, 1969.

51. Shipman, K. W. and Wood, E. R., "A Two-dimensional Theory for Rotor Blade in Forward Flight," Journal of Aircraft, Vol. 8, No. 12, December 1971, pp. 1008-1015.

52. Rao, B. M. and Jones, W. P., "Application to Rotary Wings of a Simplified Aerodynamic Lifting Surface Theory for Unsteady Compressible Flow," Proceedings of the AHS/NASA-Ames Specialist's Meeting on Rotorcraft Dynamics, February 1974.

53. Kocurek, J. D. and Tangler, J. L., "A Prescribed Wake Lifting Surface Hover Performance Analysis," Preprint No. 1001, Presented at the 32nd Annual National V/STOL Forum of the American Helicopter Society, Washington, D.C., May 1976.

54. Elchuri, V., "Prediction of Unsteady Loads and Moments on Ship Propellers," Ph.D. Dissertation, Texas A&M University, August 1977.

55. Schatzle, P. R. "Unsteady Airloads on Rotary Wings in Subsonic, Compressible Flow," M.S. Thesis, Texas A&M University, May 1976.

56. Rao, B. M. and Schatzle, P. R., "Analysis of Unsteady Airloads of Helicopter Rotors in Hover," Presented at the AIAA 15th Aerospace Sciences Meeting, AIAA Paper No. 77-159, January 1977 (Also to be published in the Journal of Aircraft).

57. Bartsch, E. A., "In-Flight Measurements and Correlation with Theory of Blade Airloads and Responses on the XH-51A Compound Helicopter Rotor - Volume I: Measurement and Data Reduction of Airloads and Structural Loads," USAAVLABS TR-68-22A, May 1968.

58. Friedman, P. and Yuan, C., "Effect of Modified Aerodynamic Strip Theories on Rotor Blade Aeroelastic Stability," Proceedings of the AIAA/ASME/SAE 17th Structures, Structural Dynamics and Materials Conference, May 1976, pp. 398-411.

59. McQuien, L. J., "Aeroelastic Analysis of Helicopter Rotor," M.S. Thesis, Texas A&M University, December 1977.